LIQUID METAL RECONFIGURABLE ANTENNAS

A Thesis

By

HONG PAN

Submitted to the Office of Graduate and Professional Studies of
Texas A&M University
in partial fulfillment of the requirements for the degree of

MASTER OF SCIENCE

Chair of Committee,	Gregory H. Huff
Committee Members,	Robert D. Nevels
	Jean-Francois Chamberland
	Richard J. Malak
Head of Department,	Miroslav M. Begovic

August 2016

Major Subject: Electrical Engineering

ABSTRACT

This thesis work is focused on the investigation of reconfigurable antennas enabled by non-toxic liquid metal, Eutectic Gallium Indium (EGaIn). The research goal is to demonstrate the integration of emerging additive manufacturing techniques and liquid metal fluidic systems in the design of reconfigurable antennas. Three antennas have been built to demonstrate the utility of EGaIn, capability of additive manufacturing techniques, and integration of an antenna to a low cost PCB with readily available fabrication process. The first antenna is a polarization reconfigurable slot antenna backed by circular substrate integrated waveguide cavity that uses EGaIn in a microfluidic channel to change its polarization by changing the position of the aperture. The second antenna is a frequency reconfigurable dipole antenna that uses EGaIn as a radiating element to change its resonance frequency by contracting and expanding the length of EGaIn. The third antenna is a polarization reconfigurable cross patch antenna that uses EGaIn as a switch to alter its polarization. It is found that the actuation of the EGaIn in a micro-vascular channel largely depends on the size of the channel if pressure driven method is used. Incorporating EGaIn in an antenna design is capable of producing unique and versatile functionalities, and EGaIn is well suitable for reconfigurable antenna design like the ones demonstrated in this thesis work.

DEDICATION

To my family

ACKNOWLEDGEMENTS

I would like to give special thanks to Dr. Gregory Huff for his great patience and extensive support throughout my college career.

Thanks also go to my colleagues, Anthony Griffin from University of Illinois at Urbana-Champaign, the team from Air Force Research Laboratory at Dayton, Ohio, and my friends from Huff Research Group who have helped to move this research project forward. I also want to extend my gratitude to all the faculty members from Texas A&M University Electrical and Computer Engineering department who have provided great educational experience.

Finally, thanks to my mother and father for their encouragement and to my wife for her patience and love.

NOMENCLATURE

SIW	Substrate Intergrated Waveguide
PCB	Printed Circuit Borad
EM	Electromagnetic
TE	Transverse Electric
TM	Transverse Magnetic
PEC	Perfect Electric Conductor
HPBW	Half Power Beamwidth
MEMS	Micro-electro-mechanical Switch
EGaIn	Eutectic Gallium Indium

TABLE OF CONTENTS

Page

Page

LIST OF FIGURES

Page

Page

Page

LIST OF TABLES

Page

CHAPTER 1

INTRODUCTION

1.1 Introduction

Reconfigurable antennas with polarization diversity enables frequency resuse for the wireless applications in the crowded frequency specturm and improve signal reception in multipath fading environment[1]. The switching mechasim that enables polarization reconfigurable come in many flavors. Using PIN diode and varactor has the advantage of low cost and fas switching. Micro-electromechanical switch (MEMS) offers low resistance and parasitic capacitance[2, 3]. An alternative is to use liquid metal as a reshapable conductor to reconfigure the polarization. Liquid metal, mercury, has found its applications in many electronic devices (e.g. electrical switches, batteries, lamps etc.) despite its high level of toxicity[4]. Eutectic Gallium Indium(EGaIn) is emerging as an alternative because of its physical similarity to mercury and low toxicity [5]. Applications of EGaIn in RF and Microwave frequency range have been reported over the years (e.g. frequency tunable patch antenna, reconfigurable bandstop filter) [6, 7]. The success of moving EGaIn in a micro-fluidic channel with minimum residue of Gallium oxide has also been reported in [8].

This thesis work is focused on the investigation of reconfigurable antennas enabled by non-toxic liquid metal, Eutectic Gallium Indium (EGaIn). The research goal is to demonstrate the integration of emerging additive manufacturing techniques and liquid metal fluidic systems in the design of reconfigurable antennas. Three antennas have been built to demonstrate the utility of EGaIn, capability of additive manufacturing

techniques, integration of an antenna to a low cost PCB with readily available fabrication process, and high strength multifunctional structural composite. The first antenna is a polarization reconfigurable circular substrate integrated waveguide cavity backed slot antenna that uses EGaIn in a microfluidic channel to change its polarization by changing the position of the aperture. The second antenna is a frequency reconfigurable sinusoidal dipole antenna that uses EGaIn as a radiating element to change its resonance frequency by contracting and expanding the length of EGaIn. The last antenna is a polarization reconfigurable cross patch antenna that uses EGaIn as a switch to alter its polarization. Detailed design steps are provided for the slot antenna and the substrate integrated waveguide cavity. Simulation results are compared to measured results for all three antennas to verify the work performed.

CHAPTER 2

BACKGROUND AND LITERATURE REVIEW

2.1 Substrate Intergrated Waveguide Cavity

A circular waveguide cavity (Figure 1) is an air-filled or dielectric-filled metal cylinder with both ends covered by metal. Resonant frequency of the cavity (TE and TM modes) is determined by Equation (2.1) and (2.2), where c is the speed of light in free space, μ_r is the relative permeability, and ε_r is the relative permittivity, p_{nm} is the root of Bessel functions of first kind, and p'_{nm} is the root of the derivative of Bessel function of first kind. Subscript letters n, m, l indicate the cavity mode, and they can only take on integer values[9].

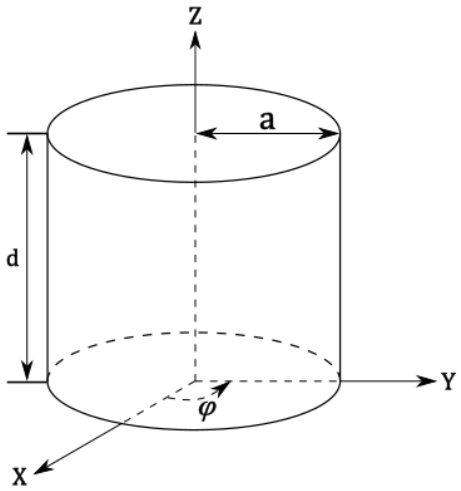

Figure 1: Circular Waveguide Cavity

TE_{nml} Mode

$$f_{nml} = \frac{c}{2\pi\sqrt{\mu_r\varepsilon_r}}\sqrt{\left(\frac{p'_{nm}}{a}\right)^2+\left(\frac{l\pi}{d}\right)^2} \tag{2.1}$$

TM_{nml} Mode

$$f_{nml} = \frac{c}{2\pi\sqrt{\mu_r \varepsilon_r}}\sqrt{\left(\frac{p_{nm}}{a}\right)^2 + \left(\frac{l\pi}{d}\right)^2} \tag{2.2}$$

Circular Substrate Intergrated Waveguide(SIW) Cavity is usually built on a thin Printed Circuit Board(PCB) substrate (e.g. 62mil). Instead of having solid cylindrical metal wall, circular SIW cavity uses via posts like the ones in Figure 2. Depending on the resonance mode in the cavity, Equation (2.1) and (2.2) are vaild if spacing, s, is much smaller than one wavelength, λ, (e.g. $s < \frac{\lambda}{10}$). The spacing between the via posts is acting like a slot in the metal wall, if the slots are parallel to the direction of current flow inside the cavity, RF energy is contained in the circular SIW cavity, and only minor cavity mode pertubation occurs[10].

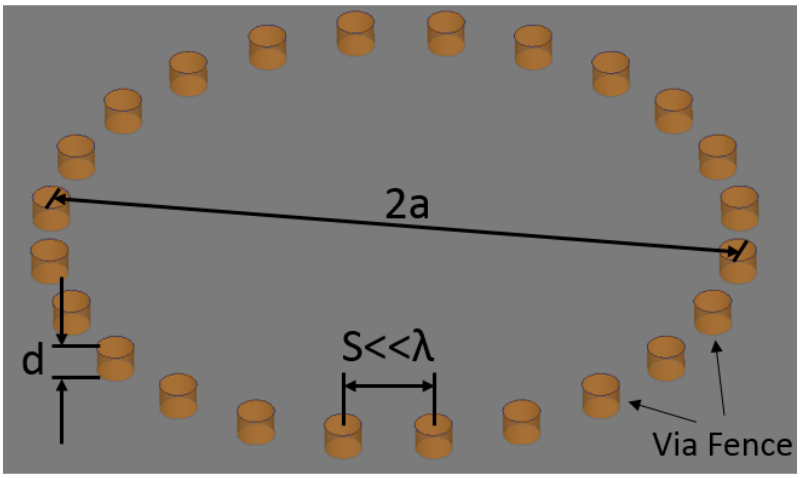

Figure 2: Example of Circular SIW Cavity

2.2 Antenna Characterization

An antenna is a one-port reciprocal device that radiates electromagnetic(EM) signal in the same way it receives the signal. Antennas are characterized by the following but not limited to: input impedance, operating frequency, bandwidth, polarization, efficiency, and radiation pattern. Antennas can be modeled as a complex impedance Z_A in a RF circuit. Z_A is the ratio of the voltage and current at the input terminal of the antenna as in Figure 3, and the real part of Z_A is composed of radiation resistance R_r and loss resistance R_L of the antenna. Loss resistance comes from the resistance of the conductor and conductance of the dielectric material. The maximum power transfer occurs when Z_A is conjugate matched to generator impedance (i.e. $R_A = R_g$ and $X_A = -X_g$). The radiation efficiency e_r is defined as the ratio of radiated power to the power delivered to the antenna, and it is related to R_r and R_L in Equation (2.5).

$$Z_A = R_A + jX_A \tag{2.3}$$

$$R_A = R_r + R_L \tag{2.4}$$

$$e_r = \frac{R_r}{R_r + R_L} \tag{2.5}$$

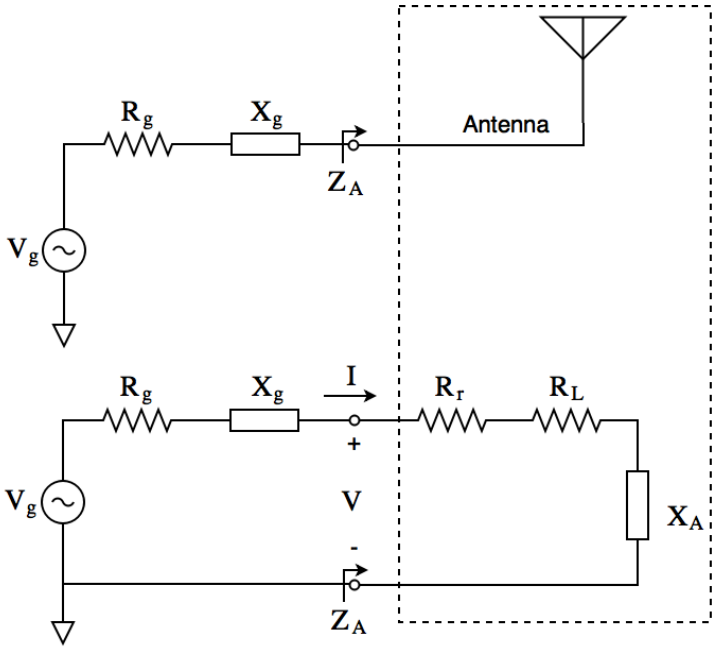

Figure 3: Antenna Circuit Model

S_{11} is a measure of reflection for a one-port device (e.g. antenna). It is the identical to reflection coefficient Γ for an antenna. Equation (2.6) is used to calculate S_{11} when load impedance Z_L and system impedance Z_0 are known[11]. Z_L is equivalent of antenna input impedance. The smaller the reflection, the more energy is delivered to the antenna. When the input impedance is conjugate matched to the system impedance(i.e. $Z_L = Z_0^*$), all the energy that is available to the antenna will be delivered to the antenna.

$$S_{11} = \Gamma = \frac{Z_L - Z_0}{Z_L + Z_0} \tag{2.6}$$

Smith chart (Figure 4) is a plot of all impedances with real part greater or equal to zero on the reflection coefficient plane[11]. The center of the smith chart represents the system impedance(usually 50ohms). Inductance sits on the upper half of the smith

chart, whereas capacitance is mapped to the lower half of the smith chart. The real and imaginary part of the S_{11} can be measured by Programmable Network Analyzer (PNA). The S_{11} data can be mapped onto smith chart using Equation (2.6) with some mathmatic manipulation.

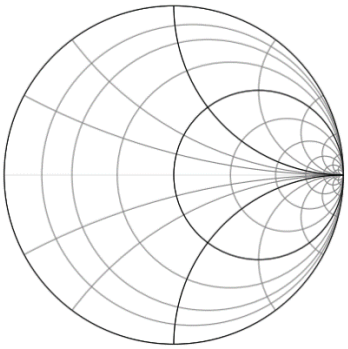

Figure 4: Smith Chart

If S_{11} magnitude is plotted in dB scale, antenna operating frequency is indicated by the lowest point of a dip for a narrow-band antenna when it is resonating. The bandwidth is found using Equation (2.7), where f_{upper} is the upper limit of the frequency with S_{11} magnitude below -10dB, and f_{lower} is the lower limit of the frequency with S_{11} magnitude below -10dB[11].

$$Bandwidth = f_{upper} - f_{lower} \tag{2.7}$$

Radiation power pattern is a graphical representation of the power radiated by an antenna in the far field. For a linearly polarized antenna, two principle cut planes from the complete 3D radiation pattern are usually used to represent the pattern. One of the

principle cut planes is E-plane because the electric field vector lays on the E-plane. The second cut plane is perpendicular to the E-plane, and it is refered as H-plane because the magnetic filed vector lays on the H-plane[12]. The power pattern is usually plotted on logarithmic scale, and it is usually normalized to the maximum value from the two cut planes. There are usually two traces plotted together in one cut plane as in Figure 5. The blue trace is the E field vector pointing in φ direction, and it is the co-polarization(co-pol) in this case. The red trace is the E field vector point in the θ direction, and it is the cross-polarization(cross-pol).

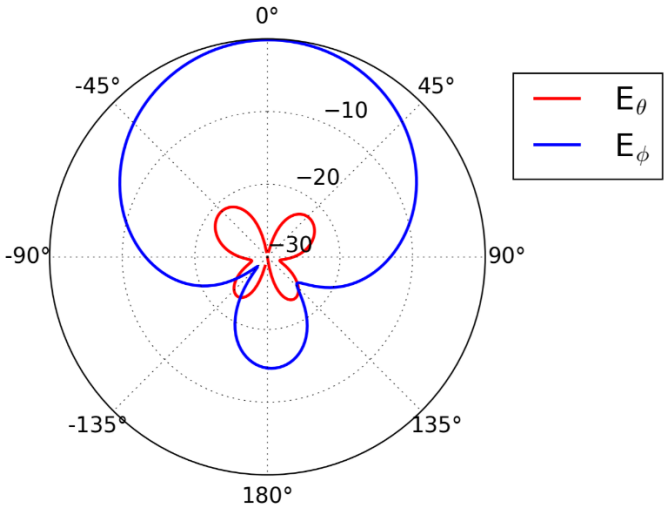

Figure 5: Radiation Pattern in dB Scale

Antenna polarization is the polarization of the EM wave emitted or received by the antenna. EM wave polarization is a figure traced out by the tip of the electric field vector in time domain at a fixed location[12]. There are linear, circular, and elliptical polarizations. This project is only concerned with linear polarization. The electric field is

linearly polarized if the vector is constrained to change in a straight line. If the receiver antenna polarization does not match to the transmitter antenna polarization, or vice versa, polarization loss occurs and is characterized by the polarization mismatch factor, $p_{loss} = |\cos(\theta)|^2$, where θ is the angle between the misaligned electric field vectors[13]. Figure 6 is an example of a linearly polarized electric field traveling in z direction.

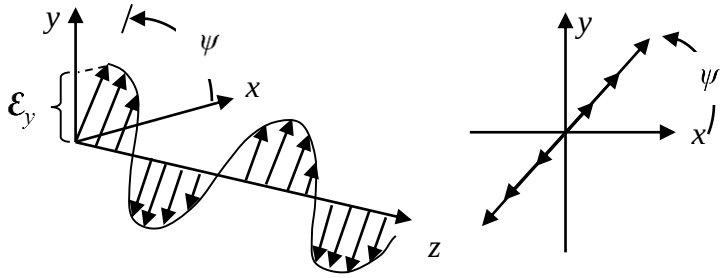

Figure 6: Example of a Linearly Polarized Wave

3dB beamwidth is a measure of angular separation between the points of 3dB power drop from the pattern maximum. It is also refered to as Half Power Beam Width(HPBW) because 3dB power drop in logrithmetic scale corresponds to half power drop in normal scale[13]. Figure 7 illusrtates the definition of HPBW of a radiation pattern in rectangular plot.

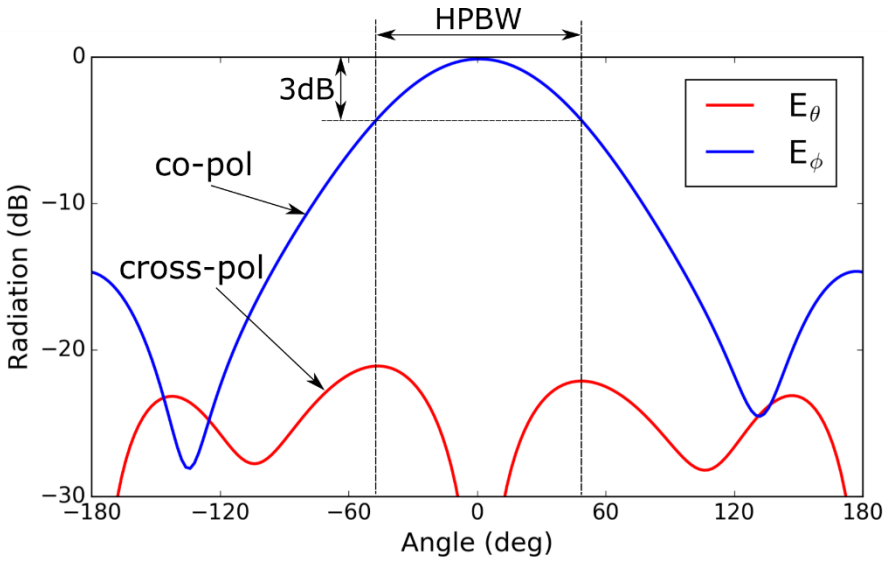

Figure 7: 3dB Beamwidth

Directivity (D) is defined as “the ratio of the radiation intensity on a given direction from the antenna to the radition intensity average over all directions.” Directivity is default to the direction in which maximum radiation occurs if no direction is given[13]. Directivity is usually in reference to an isotropic source. An isotropic source radiates the same amount of power in all direction(i.e. D = 1). Direcivity is a measure of an antenna’s ability to focus its power in a certain direction. 3dB beamwidth is narrower if directivity is higher.

2.3 Slot Antenna

A slot antenna is a linearly polarized low-profile aperature antenna. It can be realized with many geometrical configuration like rectangular, circular, elliptical shapes etc. It is popular in applications where aerodynamic profile is critical(e.g. space craft) because the apperture can be filled with dielectric material such that the opening has

smooth surface, then the overall structure can be concealed or embeded within a metal structure. One easy way to analyze the slot antenna is to analyze its complementary structure through the use of Babinet's Principle. The cut-out area is replaced by a perfect electric conductor(PEC) with the same shape and size as in Figure 8. If the PEC sheet is infinite in size, the radiation pattern of the slot antenna is the same as the pattern produced by its complementary structure except electric field and the magnetic field vector position are swapped with the magnetic filed vector position of its complementary structure[13].

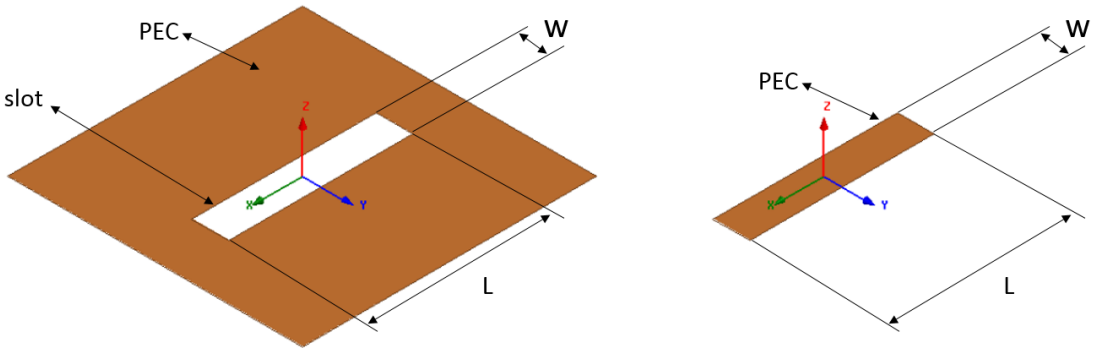

Figure 8: Slot and Its Complementary Structure

The input impedance of the two structure is related by Equation (2.8)[13], where Z_C is the input impedance of the complementary structure, Z_S is the input impedance of the slot antenna, and η is the intrinsic impedance of the medium that the antenna operates in.

$$Z_C Z_S = \frac{\eta^2}{4} \tag{2.8}$$

2.4 Half-wave Dipole Antenna

A thin half-wave dipole antenna has a sinusoidal current distribution with maximum current amplitude located at the center. The current distribution can be used to derive the radiation pattern and input impedance analytically with very close results to full wave simulated results. A half-wave dipole is inductive, and when it is in resonance, it has a length is slightly less than half-wave length, and the input impedance is about 70Ω, and the radiation pattern can be determined from Equation (2.9).

$$F(\theta) = \frac{\cos(\frac{\pi}{2}\cos\theta)}{\sin\theta} \tag{2.9}$$

2.5 Microstrip Patch Antenna

Microstrip patch antenna (Figure 9) is a metallic patch printed on top of a thin substrate (usually less than 0.05λ). The radiating mechanism is the fringing electric field along the edge of the patch as indicated by the red arrows in Figure 9. The fringing field on each side of the patch looks just like the electric field distribution in a slot antenna; therefore, analysis of a patch antenna is equivalent of analyzing two slot antennas spacing by a distance L. Equation (2.10) to (2.13) is a good starting point for calculate the length and width for a full wave simulation[12]. The physical length L in Equation (2.13) is less than $\frac{\lambda}{2}$ because the fringing field is also acting like a field in a capacitor. If the two slot antennas were to be modeled as a complex impedance, then patch length L can be modeled as a transmission line. Having a capacitor (a model from fringing field)

in series with a transmission line is equivalent of adding extra length to the transmission line; therefore, $2\Delta L$ is subtracted from physical length L to give the patch an effective electrical length of $\frac{\lambda}{2}$.

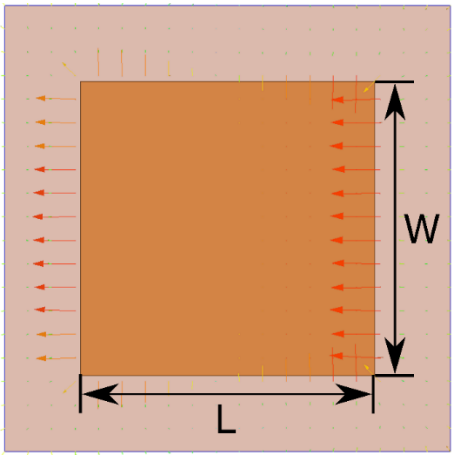

Figure 9: Microstrip Patch Antenna

$$W = \frac{c}{2f}\sqrt{\frac{2}{\varepsilon_r + 1}} \tag{2.10}$$

$$\varepsilon_{eff} = \frac{\varepsilon_r + 1}{2} + \frac{\varepsilon_r - 1}{2}[1 + 12\frac{h}{W}]^{-\frac{1}{2}} \tag{2.11}$$

$$\Delta L = 0.412h\frac{(\varepsilon_{eff} + 0.3)(\frac{W}{h} + 0.264)}{(\varepsilon_{eff} - 0.258)(\frac{W}{h} + 0.8)} \tag{2.12}$$

$$L = \frac{c}{2f\sqrt{\varepsilon_{eff}}} - 2\Delta L \tag{2.13}$$

2.6 3D Printing and Bonding

3D printing and bonding for the circular SIW cavity backed slot antenna and micrstrip cross patch antenna is a collaborative work with a team from University of Illinois at Urbana-Champaign. The following steps are taken to form microfluidic channel and bonding the channel to the PCB:

The copper of the antenna is etched using iron chloride to remove any heavy oxidation on the surface. The copper is then treated with an epoxide-functional silane which has been partially hydrolyzed. The silane is allowed to cure for 24 hours at room temperature. The epoxide functional group on the silane is to increase bonding to the cast epoxy layer.

Vascular channels were formed through the printing, embedding, and subsequent removal of a sacrificial ink. Sacrificial ink is 3D printed directly onto the antennas using a Robocaster (custom build from Aerotech). Similar to common 3D printers, the geometry and architecture of the printed ink is determined by the pressure, speed, and pre-programmed movement of the print head. Once the sacrificial ink structures and lines have been deposited on the antennas, the degassed and uncured epoxy (E8605, ε_r =2.9) is cast between the antenna and a glass plate using a 1mm thick gasket. A silicone rubber sheet (McMaster-Carr) which has been laser-cut to the precise pre-determined shape is used for the gasket, such that the epoxy will cure in this shape. The epoxy is then allowed to cure for 24 hours at room temperature, followed by a high-temperature cure cycle of 3 hours at 50 ℃ then 8 hours at 121 ℃. The high temperature cure is necessary for the epoxy to achieve its desired mechanical and thermal properties.

After the epoxy is fully cured, the glass and gasket are removed, leaving only the epoxy, sacrificial ink, and antenna. The sacrificial ink is removed, forming the vascular channels, by heating the ink to 100 ℃ (melting the ink) and extracting it with light vacuum. To remove any small amount of wax which may remain on the channel sidewalls, the channels are flushed with petroleum ether.

2.7 Structurally Embedded Microfluid Channel Fabrication

Structurally Embedded Microfluid Channel for sinusoidal dipole antenna is a collaborative work with a team from Air Force Research Laboratory at Dayton, Ohio. The steps taken to embed the channel in the composite is described in [14].

CHAPTER 3

POLARIZATION RECONFIGURABLE SIW CAVITY BACKED SLOT ANTENNA

3.1 Design and Analysis

The objective for the slot antenna project is to automate the process of moving EGaIn in a microvascular network and low cost PCB integration. The slot antenna is an antenna of choice for this project because it is easy to intergrating into a PCB. The specifiction of the slot antenna is 2.425GHz operating frequncy and 50ohms input impedance. From Baninet's principle, the complementary structure of a narrow half-wave length slot-out is approximated as a half-wave length dipole. The length(L) of the slot cut-out is calculated using Equation (3.1), where f is the resonance frequency, $\mu_r = 1$ and $\varepsilon_r = 4.4$ because FR4 is used as dielectric material of the PCB.

$$L = \frac{\lambda}{2} = \frac{c}{\sqrt{\mu_r \varepsilon_r}} \frac{1}{f} \tag{3.1}$$

To excite the slot antenna, a circular SIW cavity with 2.425GHz resonant frequency is constructed, then the slot antenna is simply a cut-out area of the SIW cavity. Acoording to [10], when current is perpendicular to the slot, large amount of engery leaks through the slot. A simple design flow is to analyze the surface current flow of the available cavity mode first, then determine the shape of the slot that cuts through the current flow perpendicuarly. The SIW cavity not only provides excitation to the slot antenna, it also isolates the slot antenna from other circuit elements on the same PCB.

TM_{010} mode is determined to be suitable because the magnetic field is circulating inside the cavity, and accoording to the boundary condition, current flow is

perpendicular to the magnetic field on the top conductor of the cavity. A rectangular slot is curved such that the slot cuts across the current flow to create maximum amount of leak of energy in the cavity. The size of the cavity is calculated using Equation (2.2).

3.2 HFSS Simulation

The parameters found in the previous analysis provides a starting point for the slot antenna structure to be simulated and fine-tuned in HFSS. A circular SIW cavity is simulated first. Figure 10 provides confirmation to the previous analysis of magnetic field and electric current flow on the top conductor of the cavity. Figure 11 shows a slot that is approximately half-wave length long intercepts the current flow of the cavity.

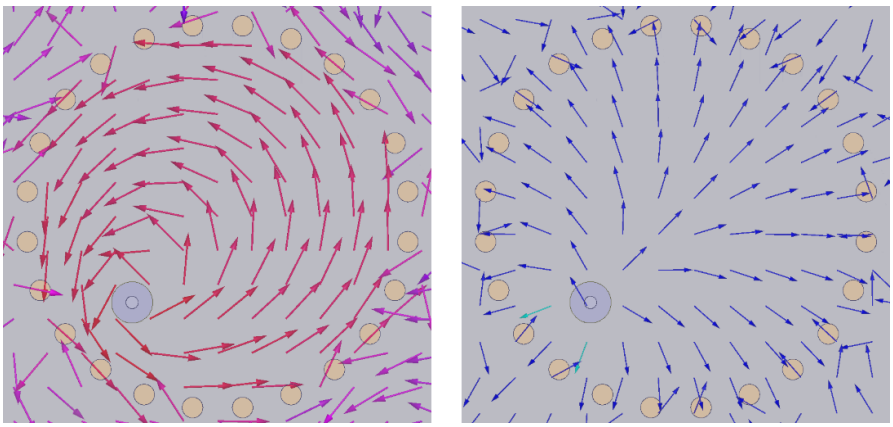

Figure 10: Circular SIW Magnetic Field (Left) and Current Flow (Right)

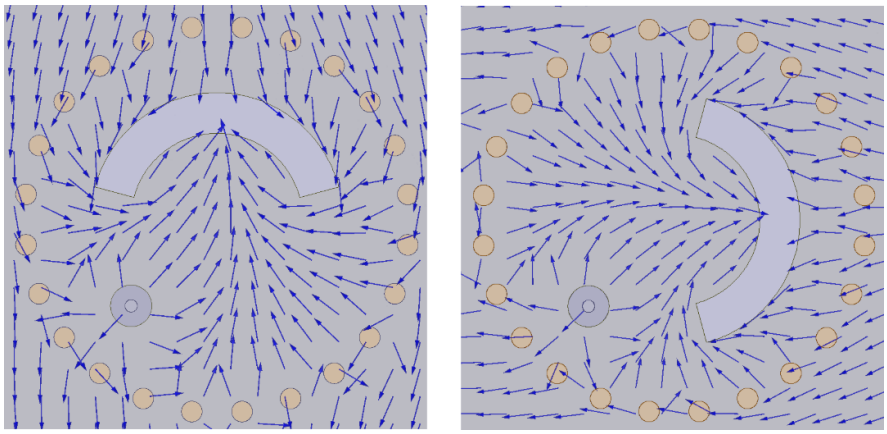

Figure 11: Current flow and Cut-out Area in the Cavity; State 1 (Left); State 2 (Right)

To construct a polarization reconfigurable slot antenna, two identical slots are created, and one of them is physically rotated by 90 degrees as in Figure 11. Then the slots are merged together to form a longer slot (Figure 12). The EGaIn that flows in a channel brings back one of the shorter slot by covering up a portion of the longer slot as in Figure 13. Because of the symmetry of the structure, when the impedance is matched in one of the states, the other state is also impedance matched when the antenna makes the transition between states.For the future discussion, polarization state of the antenna are named state 1 and state 2 as in Figure 13 .

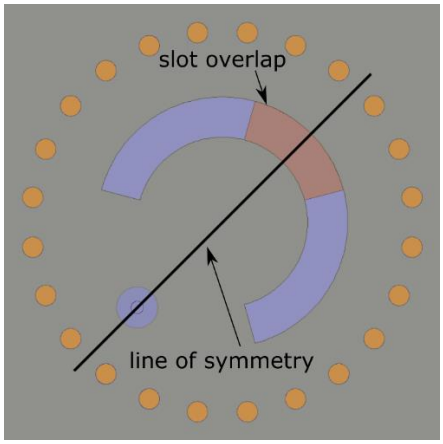

Figure 12: Merged Slot

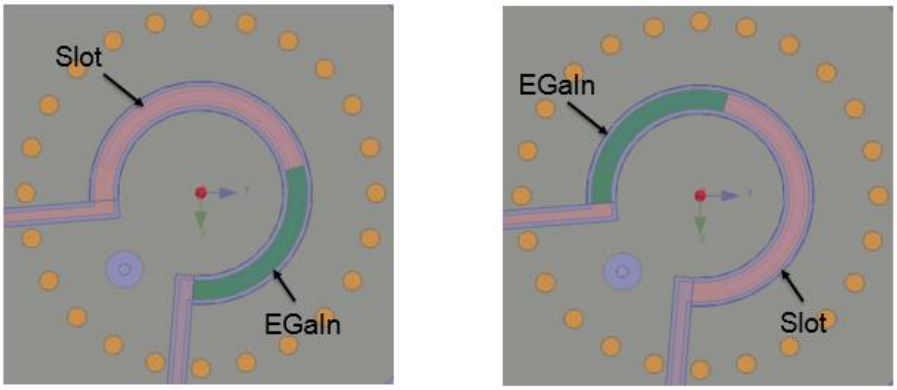

Figure 13: Slot Antenna with EGaIn

Figure 14 is a snap-shot of the 1st version of the complete slot antenna structure with channel and sensing network in HFSS. The pushing fluid is in pink, the sensing fluid (in between sensing pad 2 and pad 3) is in blue, and EGaIn is in green. All three fluids are immiscible when injected in the channel. Detailed dimension of each component is in Table 1.

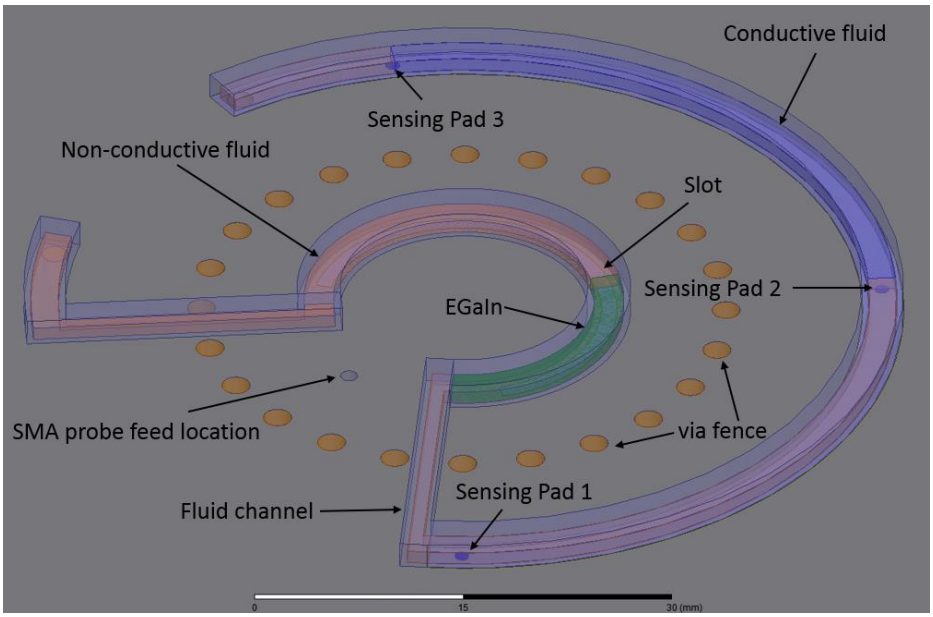

Figure 14: Version 1 Slot Antenna Structure in HFSS

The volume of the sensing fluid is set up to match the volume of EGaIn in a way that when the sensing fluid moves from in between sensing pad 2 and pad 3 to sensing pad 1 and pad 2(transitioning from state 1 to state 2), the EGaIn is moved with enough distance to reconfigure the slot antenna from state 1 to state 2. In Figure 15, EGaIn is pushed to have the same length of the slot as in state 1 appears in a different orientation as in state 2, and the polarization changes from X-directed to Y-directed.

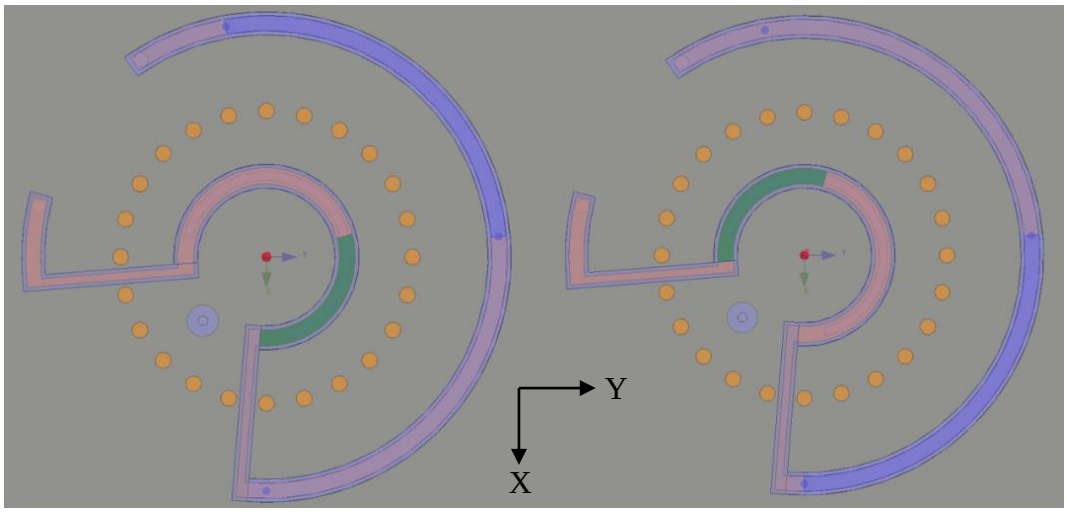

Figure 15: Version 1 State 1 (Left) Vs. State 2 (Right)

Cavity Radius	19.08
Via Size	1.0265
Slot Width	1.13
Curved Slot Length for One State	30.4
Channel Width	2.13
Channel Height	1
Probe Feed Radial Location	11.75

Table 1: Detailed Dimensions (Unit = mm)

The operating frequency of both states of the slot antenna is 2.425GHz as seen from the magnitude of S_{11} response in Figure 16. From S_{11} data plotted in smith chart in Figure 17, the input impedance for both states is matched to 50ohms. The normalized radiation patterns closely resemble an antenna with linear polarization in Figure 18 and Figure 19 because the difference between cross-polarization and co-polarization is

greater than 15dB in the 3dB beamwidth area. It is evident that the polarization is switched when transitioning from state 1 (Figure 18) to state 2 (Figure 19).

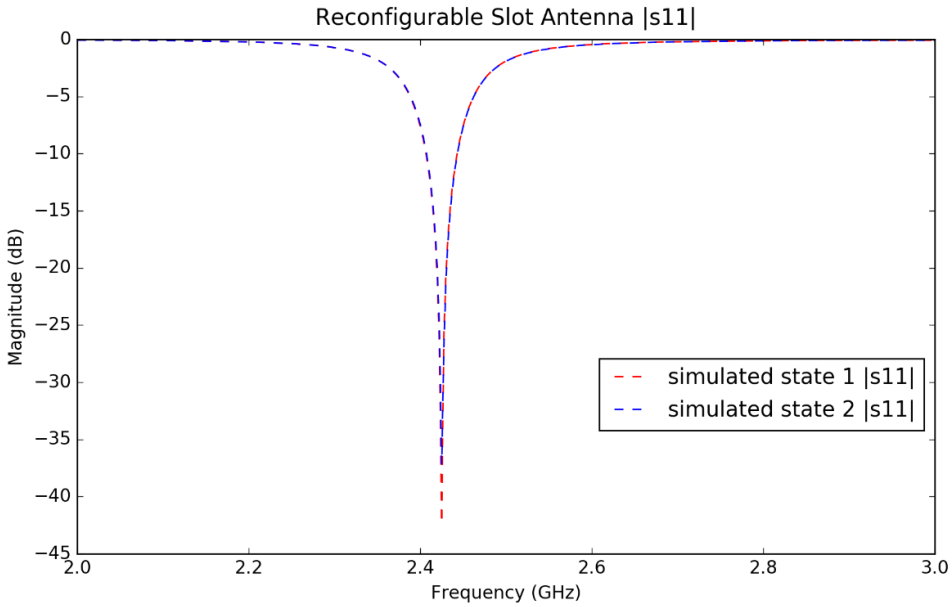

Figure 16: Version 1 Simulated $|S_{11}|$

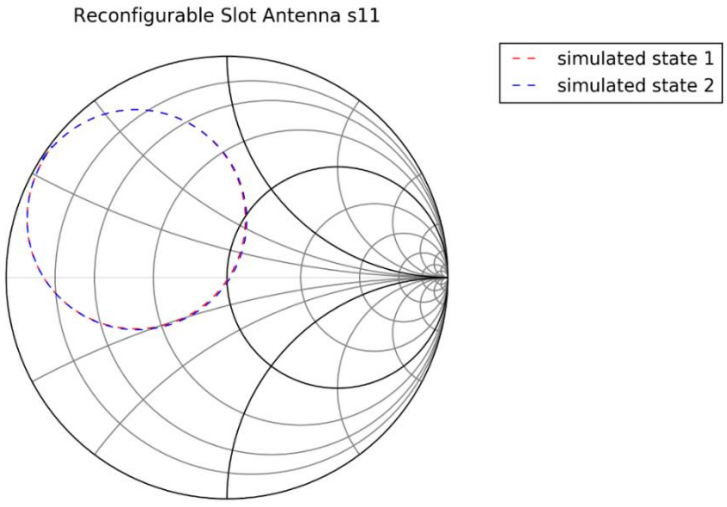

Figure 17: Version 1 Simulated Input Impedance

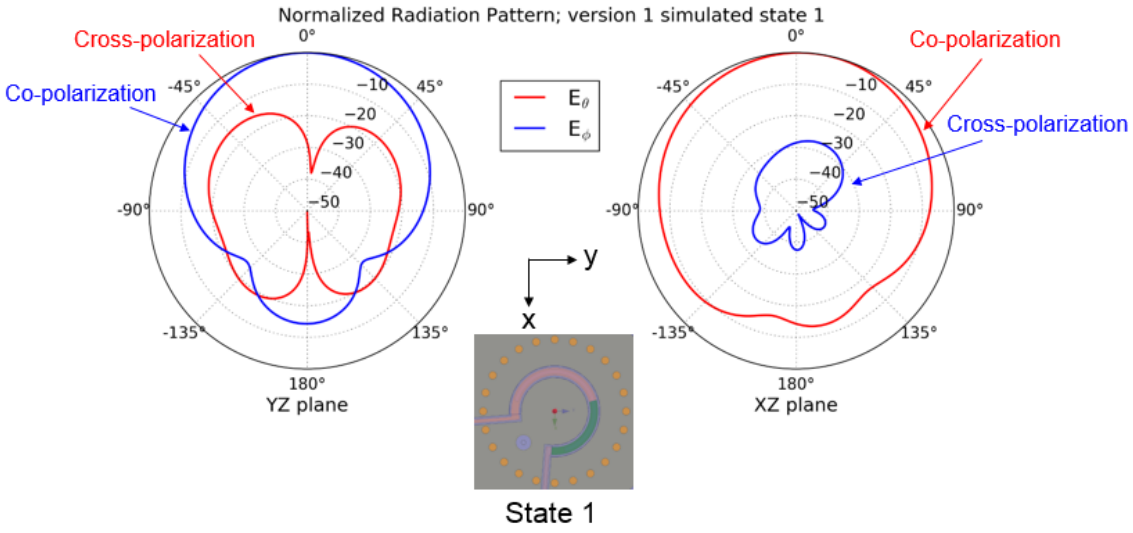

Figure 18: Version 1 State 1 Simulated Normalized Radiation Pattern

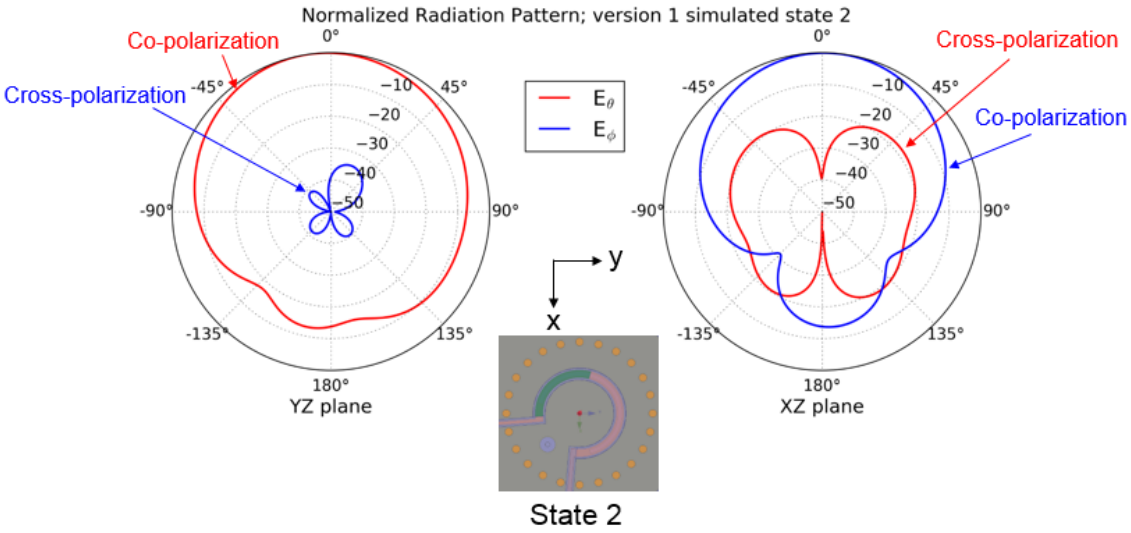

Figure 19: Version 1 State 2 Simulated Normalized Radiation Pattern

3.3 Sensing Network

In order to automate the process of reconfiguring the polarization, the slot antenna is integrated into a PCB with control circuit built around it. EGaIn is actuated using microfluid pump. A sensing network is constructed to determine the position of the EGaIn and used as a decision making signal. The sensing network consists of three copper pads. One is connected to a 5V DC, the other two are connected to the input pins of a microcontroller. Then water is used as a conducting path for the 5V signal to reach to the microcontroller. Figure 20 is a block diagram of the control network.

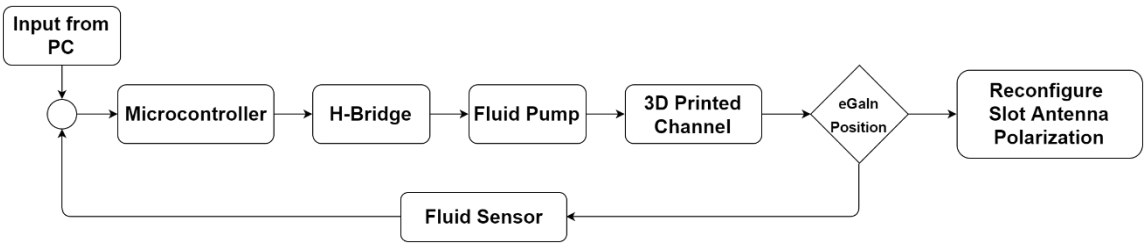

Figure 20: Control Network

3.4 Fabrication and Verification

Figure 21 is the first version of the fabricated PCB with control and sensing circuit components included. The channel is 3D printed using makerbot replicator 2 with polylactic acid filament. The constraint from 3D printing tolerance and channel bonding technique limits the channel size to be no smaller than 2mm. Figure 22 shows the state 1 and state 2 of the slot antenna with EGaIn in the channel. After trial and error, Hydrocal 2400 is the choice of the pushing fluid because of its high viscosity, and it is immiscible

with water (sensing fluid) and EGaIn. In Figure 22 state 2, the channel is pre-filled with Hydrocal 2400 and EGaIn, and it is clear of any oxidation or debris initially. When transitioning from state 2 to state 1, even though Hydrocal 2400 is viscous enough to pushing EGaIn, severe laminar flow is observed as indicated by the red circle in Figure 22, and the channel is filled with black material. Figure 23 is a picture of the black material under microscope. It is seen that the black material is the EGaIn oxidation and debris. A good VSWR response from state 2 is observed in Figure 24, but the slot antenna in state 1 fails to operate completely because of EGaIn oxidation and debris.

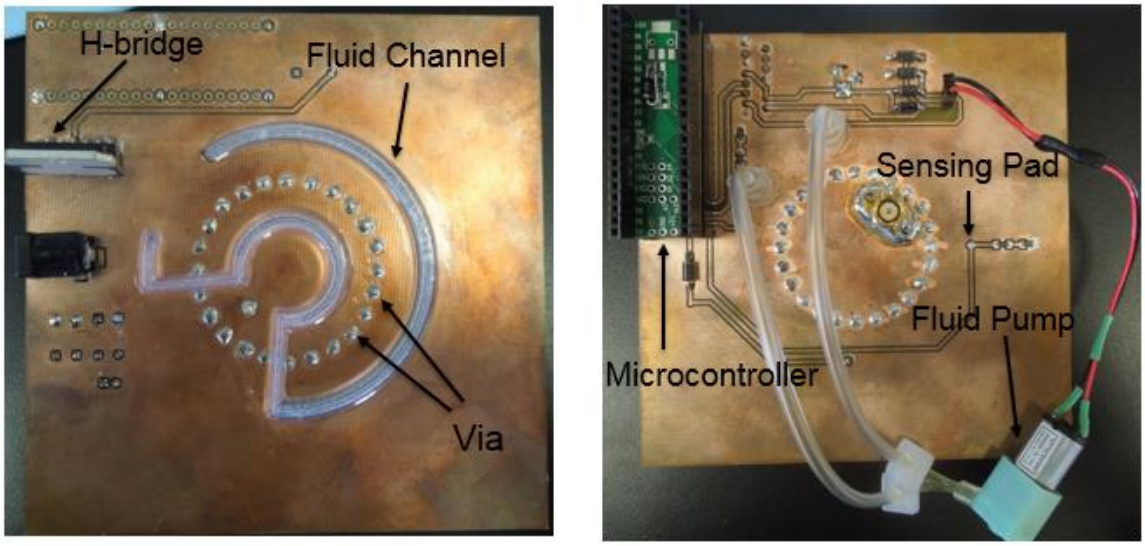

Figure 21: Fabricated Version 1

Figure 22: Fabricated Version 1 State 1 (Left) vs. State 2 (Right)

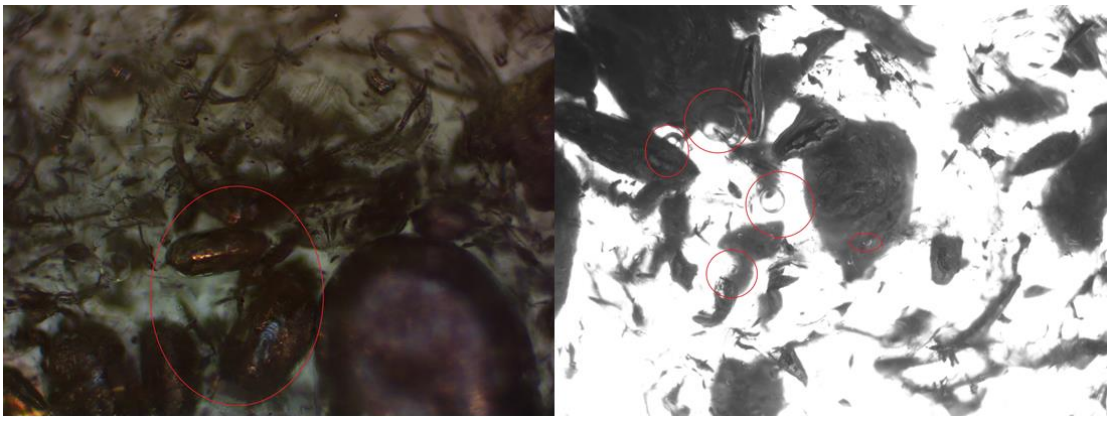

Figure 23: Version 1 EGaIn Oxidation and Debris (Left) and Air Bubble (Right)

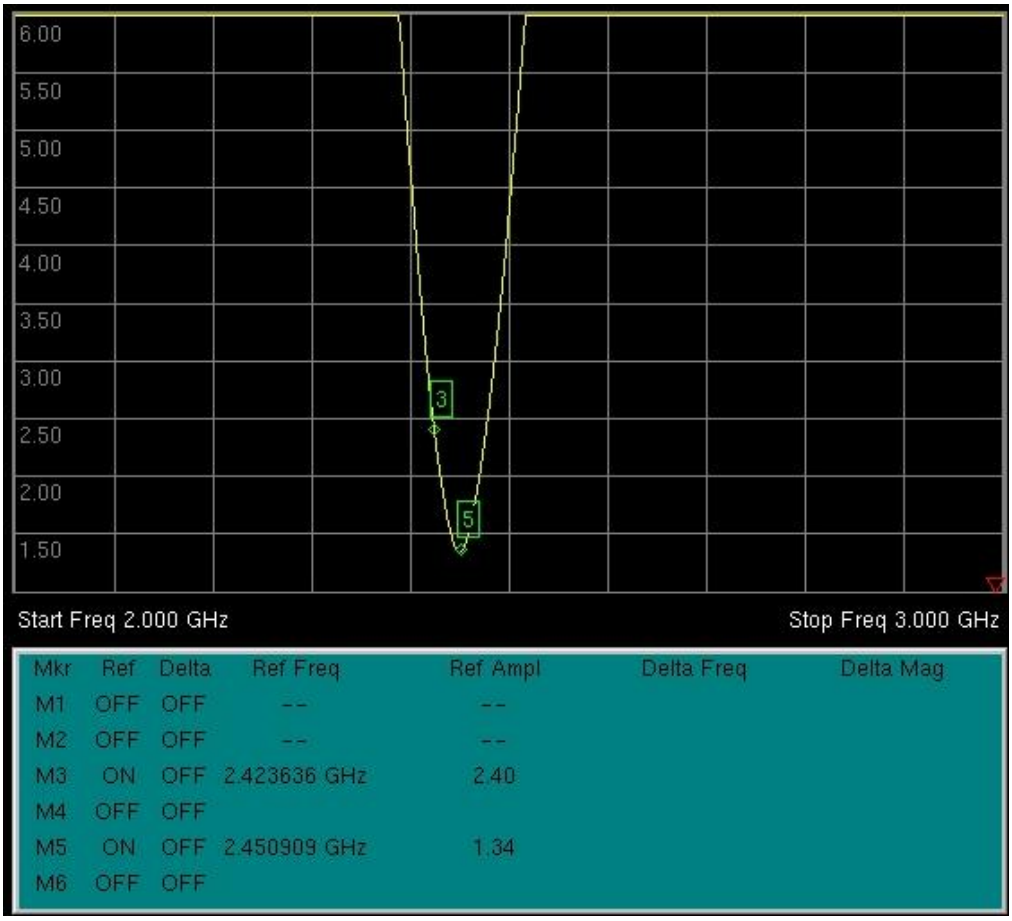

Figure 24: Version 1 State 2 Measured VSWR

The findings from version 1 lead to the second channel design which has a much smaller channel and different pushing fluid to stop laminar flow, EGaIn debris and oxidation from occurring. The new channel design is a square wave like stith going across the slot as in Figure 25.

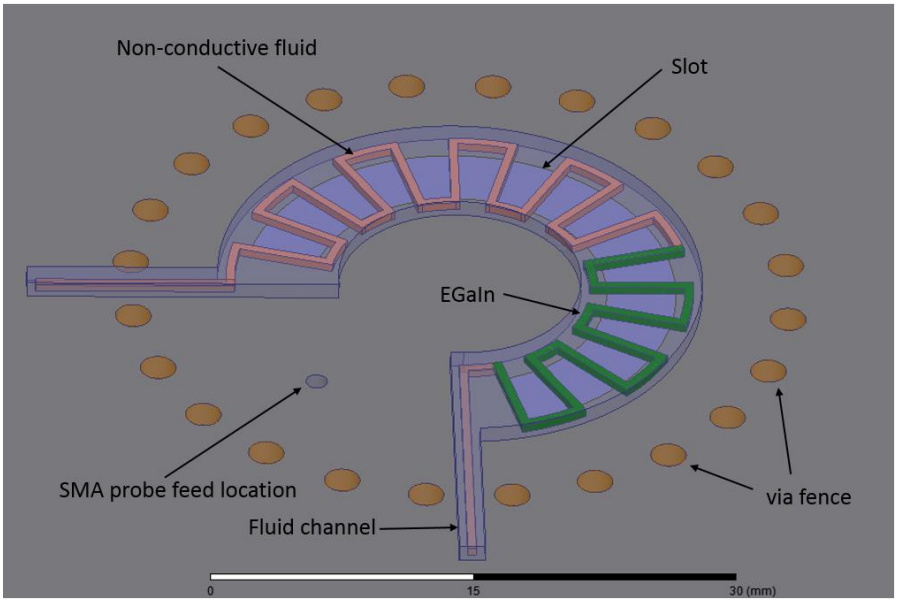

Figure 25: Version 2 Slot Antenna Structure in HFSS

The new design only requires to tune probe feed position slightly to have 50ohms input impedance. Instead of covering up the cut-out area completely as in version 1, the slot is covered up effectively. The angluar spacing of the stith is the same as the via. Table 2 is the comparison of the dimension of the channel and antenna structure between version 1 and version 2. The width and length of the channel in the 2nd version is only 0.5mm. Figure 26 shows the difference between state 1 and state 2.

Version	Slot Width	Probe Feed Radial Location	Channel Width	Channel Height
1	1.13	11.75	2.13	1
2	4	12.02	0.5	0.5

Table 2: Comparison of Dimensions in Version 1 and Version 2 (Unit = mm)

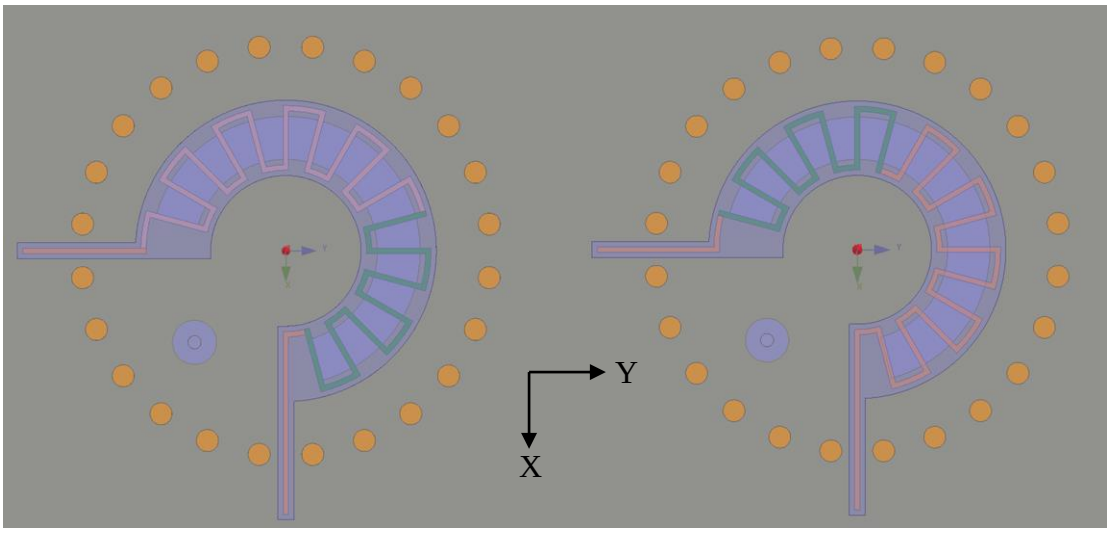

Figure 26: Version 2 State 1 (Left) Vs. State 2 (Right)

Figure 27 is the second version of the fabricated slot antenna with control circuit components fully populated. Figure 28 shows the state 1 and state 2 of the slot antenna with EGaIn in the channel. After transitioning from state 1 to state 2, EGaIn debris only accumulates at the places where the copper is present, which does not affect the operation of the slot antenna. The portion of the channel that directly goes across the slot has minimum EGaIn oxide and debris for two reasons; the first has to do with the size of channel. It is small enough to prevent laminar flow from occurring; therefore, no debris will form, and liquid with low viscosity like Fluorinert FC-70 is capable of pushing EGaIn in the channel. The second reason is the use of Fluorinert FC-70 helps to minimize the oxidation of EGaIn.

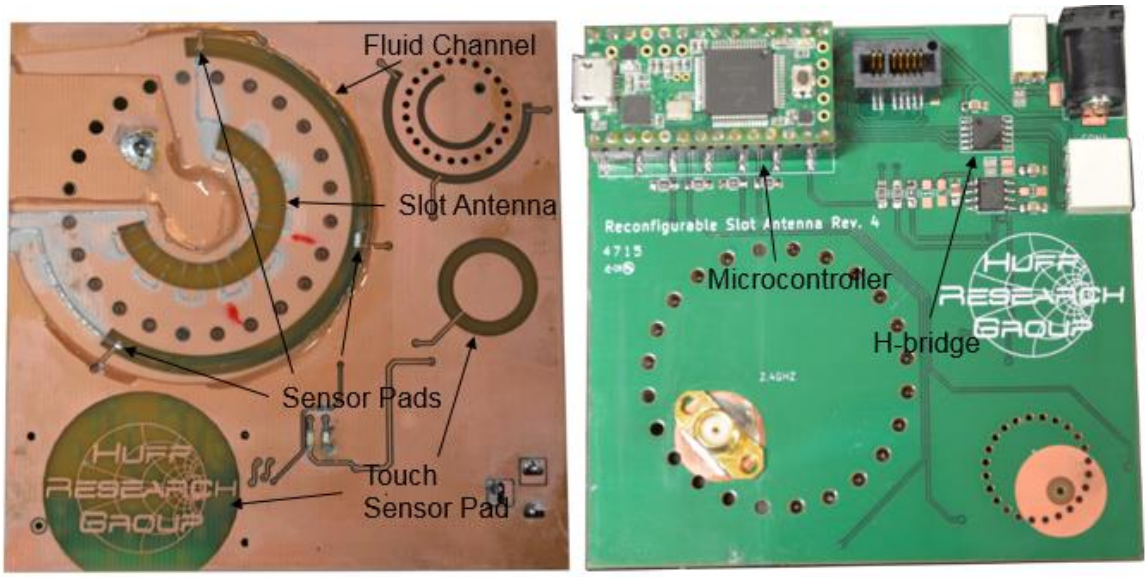

Figure 27: Fabricated Version 2

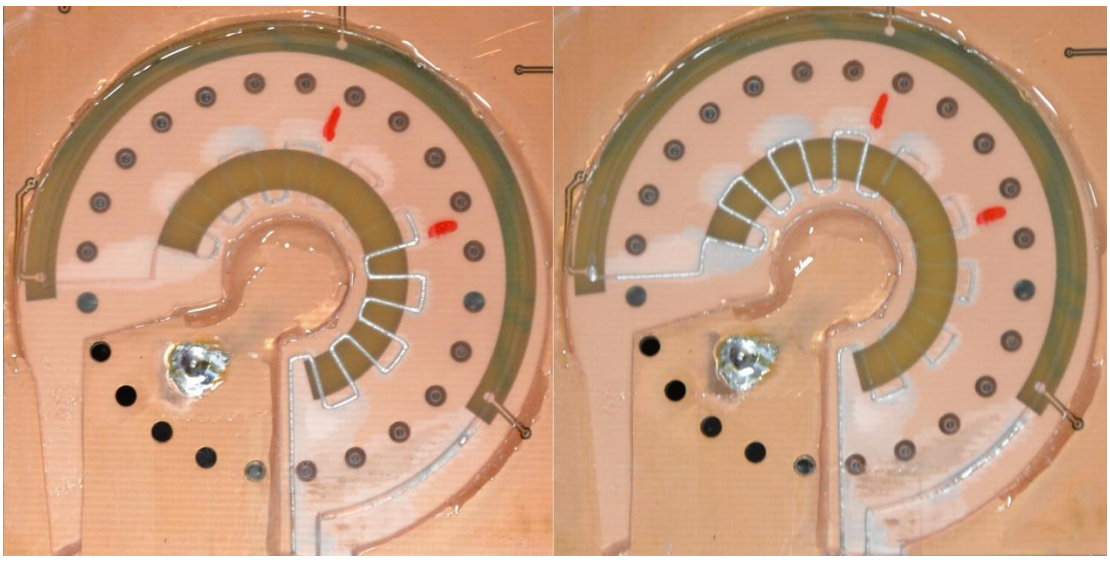

Figure 28: Fabricated Version 2 State 1 (Left) Vs. State 2 (Right)

Figure 29 is a plot of S_{11} magnitude measurement data overlaid on top of simulated data. Due to manufacturing tolerance, the slot length in state 1 is slightly

longer than the slot length in state 2 which shows up as frequency shift in S_{11} measurement. Both state 1 and state 2 resonant frequency is higher than the simulated frequency is mainly because the dielectric constant of FR4 is lower than simulation. The S_{11} data on smith chart from Figure 30 shows that both state 1 and state 2 has input impedance very close to 50ohms (the center of smith chart). The S_{11} circles are rotated in the smith chart because the feed port of the SMA connector is de-embedded with a length of the probe. During the S_{11} measurement, the network analyzer is only calibrated up to the feed port. The length of the probe acts as a transmission line, and a length of transmission line manifests itself as a rotation when S_{11} is plotted on smith chart. Table 3 is a summary of measured data compared to simulated data.

	Simulation		Measurement	
	State 1	State 2	State 1	State 2
Frequency (GHz)	2.425	2.425	2.451	2.463
2:1VSWR bandwidth (MHz)	42	42	41	41
Z_{in} (Ω)	50	50	51+5.8j	51+7.2j

Table 3: Comparison of Version 2 Simulated and Measured S_{11} Data

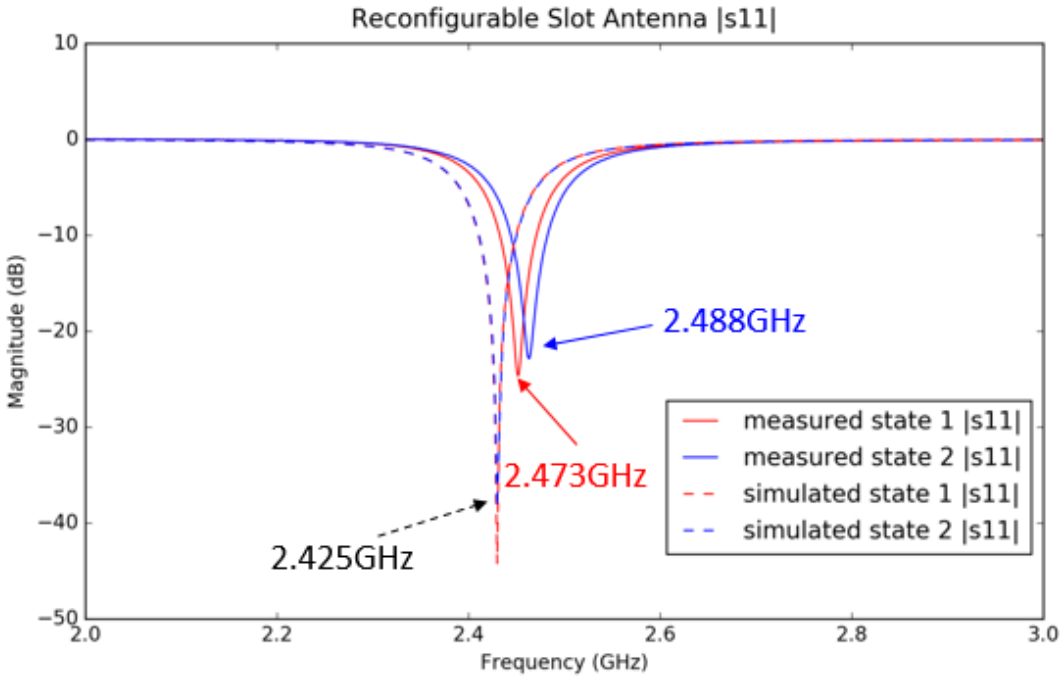

Figure 29: Version 2 Simulated Vs. Measured $|S_{11}|$

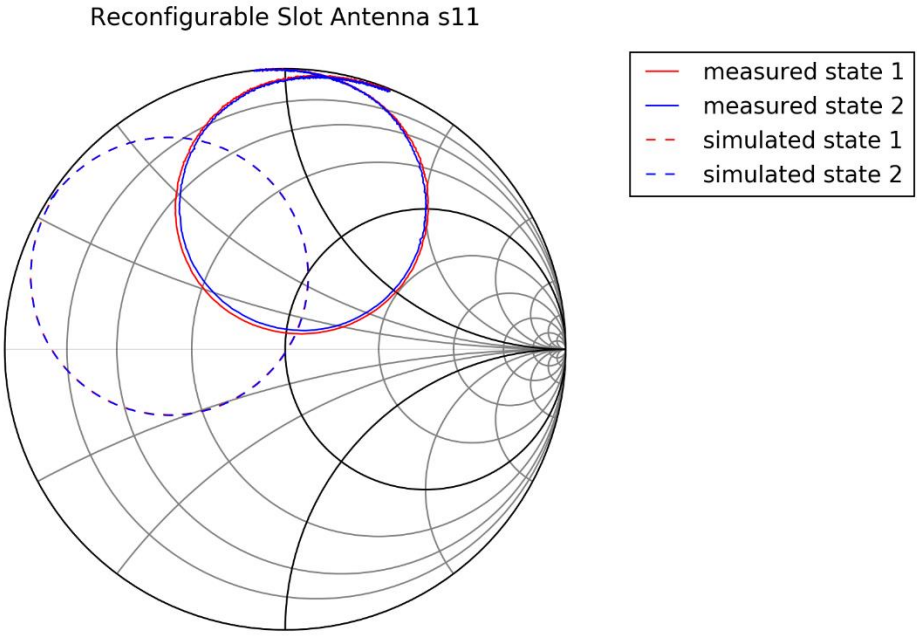

Figure 30: Version 2 Simulated Vs. Measured Input Impedance

Figure 31(state 1) and Figure 32(state 2) are the comparison between simulated and measured data of normalized radiation patterns in the principle cut planes. The shape of the measured data resembles the simulated data except the cross polarization pattern. Measured data shows that the slot antenna on the PCB has large cross polarization. Cross polarization is higher than the simulated results because of the control circuits around the antenna. Table 4 is a summary of the information extracted from radiation pattern data. The fabricated slot antenna is less directive compared to the simulation.

	Simulation				Measurement			
	State 1		State 2		State 1		State 2	
Plane	XZ	YZ	XZ	YZ	XZ	YZ	XZ	YZ
Directivity (dBi)	6.6	6.6	6.5	6.5	4.3	4.8	5.2	5.0
3dB Beamwidth (deg)	96	82	81	98	102	99	89	96
Co-Polarization	E_θ	E_ϕ	E_ϕ	E_θ	E_θ	E_ϕ	E_ϕ	E_θ

Table 4: Comparison of Version 2 Simulated and Measured Radiation Pattern Data

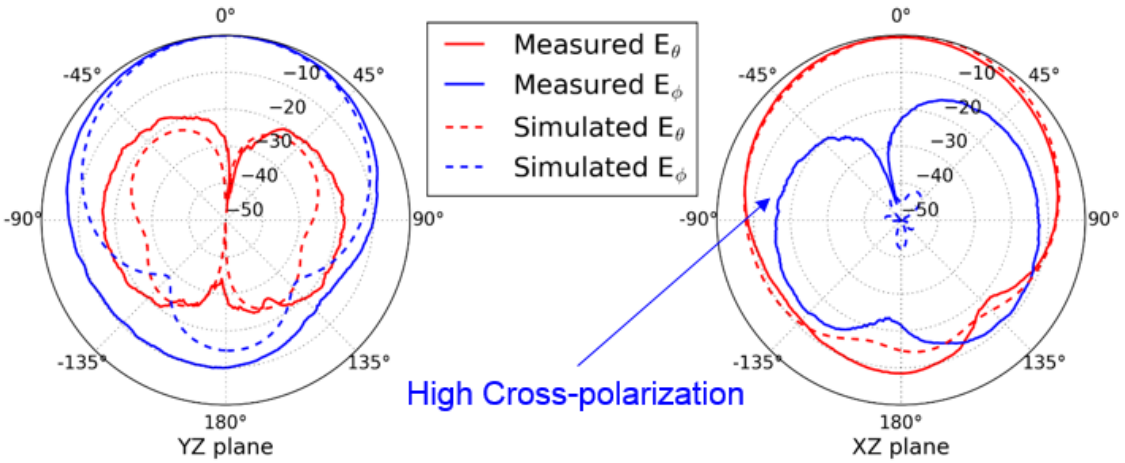

Figure 31: Version 2 State 1 Simulated Vs. Measured Normalized Radiation Pattern

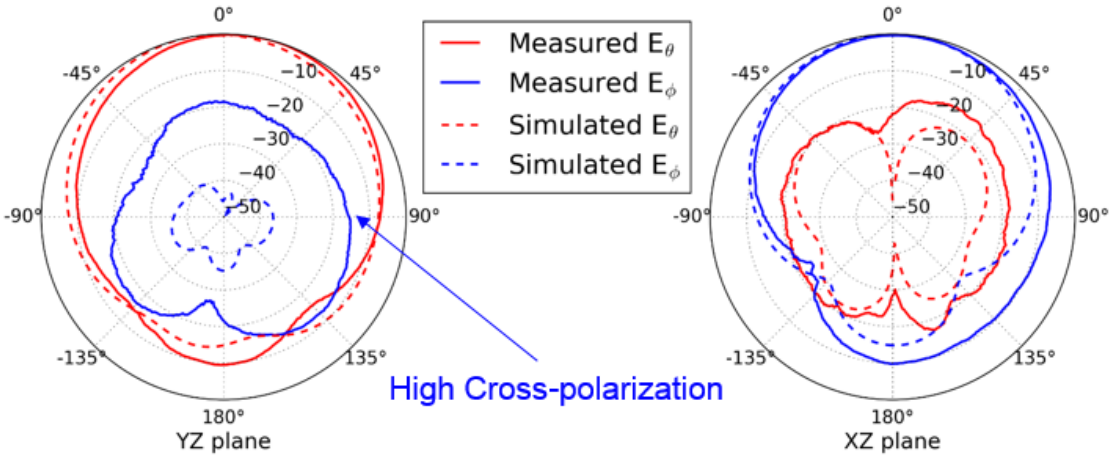

Figure 32: Version 2 State 2 Simulated Vs. Measured Normalized Radiation Pattern

To investigate the source of the high cross polarization, the slot antenna is covered up by copper tape, and the copper tape is soldered to the ground as in Figure 33. Then the radiation pattern is measured and plotted in Figure 34. The high cross polarization is still present. It makes sense because the electric field is going across a rectangular slot antenna, and if the rectangular slot is curved like the one in the current design, the electric field is curved and gives rise to the high cross polarization. The high cross polarization is evident from YZ cut plane in Figure 34, but the simulation failed to pick up the cross polarization in XZ cut plane.

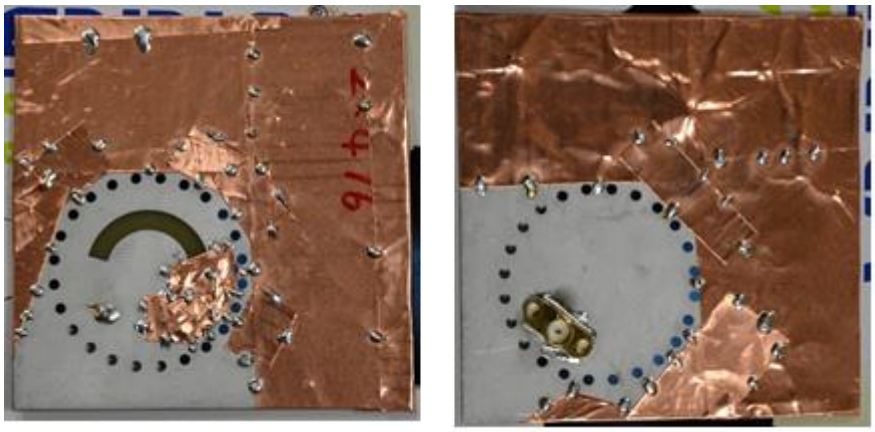

Figure 33: Slot Antenna with Ground Plane and Slot Covered by Copper Tape

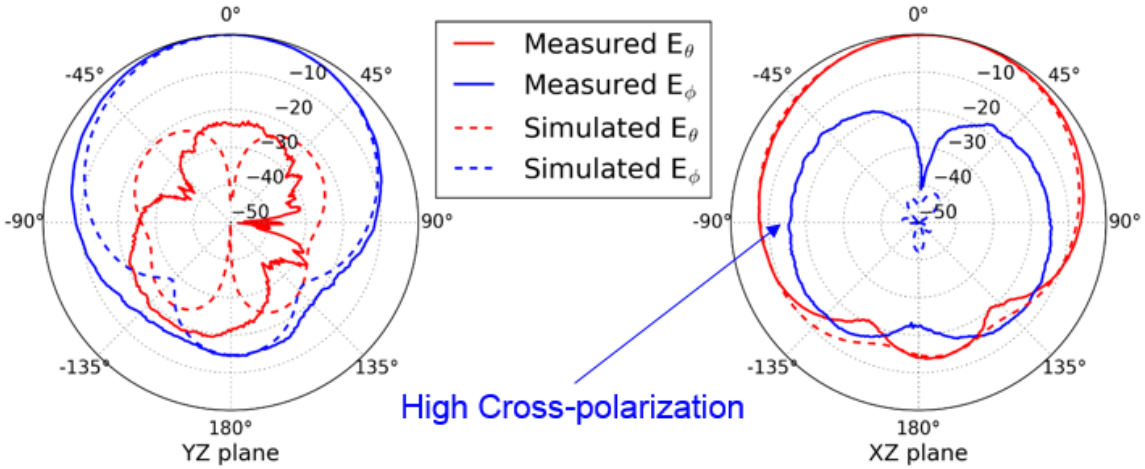

Figure 34: Measured Radiation Pattern for the Slot Antenna from Figure 33

CHAPTER 4

FREQUENCY RECONFIGURABLE SINUSOIDAL DIPOLE ANTENNA

4.1 HFSS Simulation

The objective of the sinusoidal antenna is to provide frequency tunability over a wide bandwidth and to minimize antenna installation area and/or weight for the use on an aircraft. The parameterization of the sinusoidal dipole antenna is based on a growing oscillation that follows a power-series envelope. Equation (4.1) and (4.2) are parameterized according to the maximum physical length of the dipole's meandering length in the lateral direction; this is a function of the maximum size of the composite panel in that direction and corresponds to a square panel with a length and width of 6 inches. This parameterization was chosen since it provides a smooth transition from the feed network and a gradual transition of the structure from the linear dipole expansion to the growing oscillation-based meandering growth. Figure 35 shows the HFSS model of the antenna geometry. Table 5 has the electrical properties of the dielectric materials. A more detailed view of the feed structure is illustrated in Figure 36. It consists of a double-sided parallel strip line that transitions into a short dipole. Then the dipole is connected to the EGaIn trace through the vias.

$$x(t) = 75.7mm * \left(\frac{t}{3}\right)^2 \sin\left[2.5\pi t\right] \tag{4.1}$$

$$y(t) = 75.7mm * \frac{t}{3} + 10mm \tag{4.2}$$

Material	Dielectric Constant	Loss Tangent
FR4	4.4	0.02
RM-2014-LDk	2.92	0.006

Table 5: Sinusoidal Antenna Material Electrical Properties

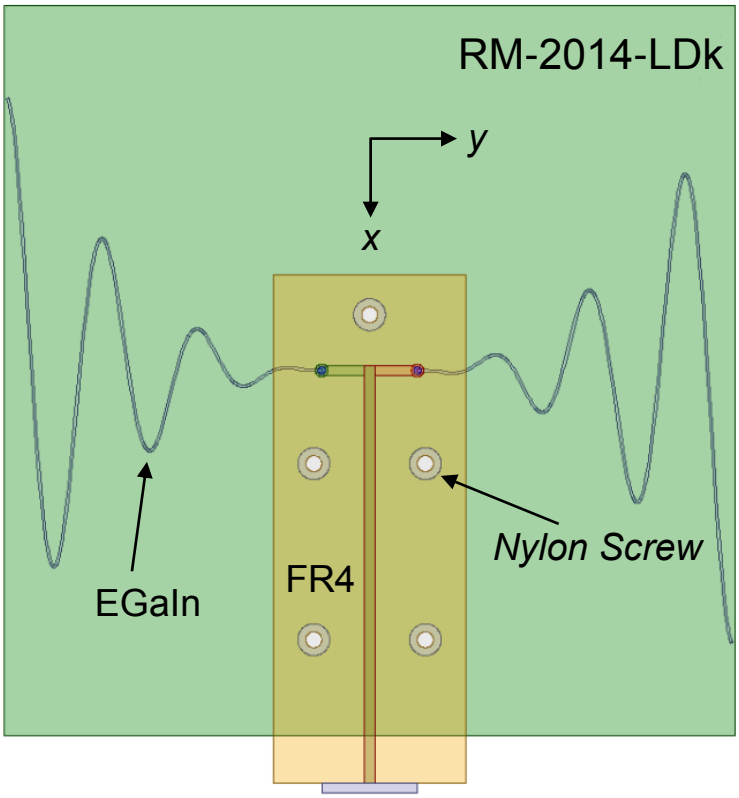

Figure 35: Sinusoidal Model in HFSS

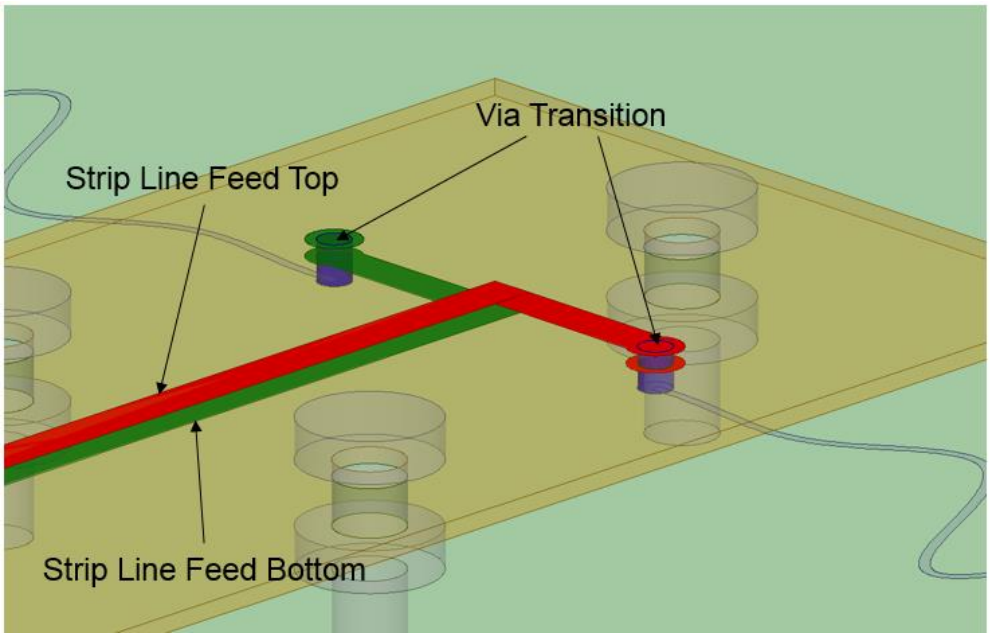

Figure 36: Sinusoidal Antenna Feed Structure

This parameterization also creates an opportunity to study the family of antennas created by altering the oscillatory and growth parameters. Equation (4.3) and (4.4) provide a version that has been 'flattened' to a linearly-expanding dipole structure. The two contour plots in Figure 38 show the log-magnitude of the antenna's input reflection coefficient (S_{11}). These were obtained by simulating the parameter t from 0 in $\leq t \leq 2.4$ in 25 mil (0.635 mm) steps. Two adaptive frequencies were simulated in Ansys HFSS with interpolating frequency sweeps discretized into 1 MHz steps; these were 10 MHz < f_0 = 1 GHz < 2 GHz and 1 GHz < f_0 = 3 GHz < 5 GHz. The overlapping region from 1 GHz to 2 GHz was transitioned using a logistic transition equation with a linearized transition region occurring over the range 1.8 GHz to 2.0 GHz; this allowed the two functions to be combined for the purpose of plotting and address discrepancies in this

overlap region (the transition range was found by inspection).

$$x(t) = 75.7mm * \left(\frac{t}{3}\right)^{20} \sin\left[2.5\pi t\right] \tag{4.3}$$

$$y(t) = 75.7mm * \frac{t}{3} + 10mm \tag{4.4}$$

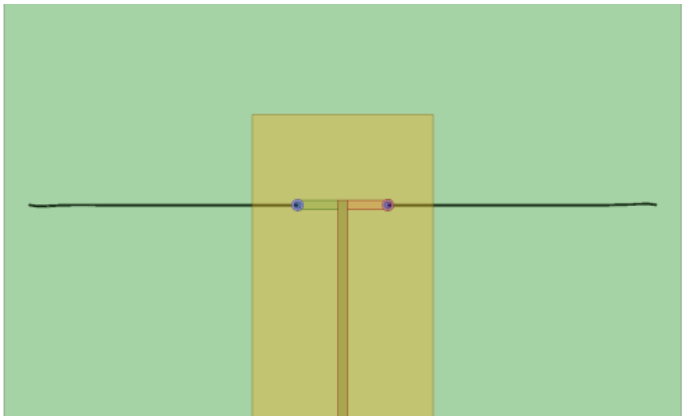

Figure 37: Straight Dipole or "Flattened" Version of the Sinusoidal Dipole Antenna

In Figure 38, x axis is the parameter t in inches, y axis is frequency in GHz, and the color of the contour plot indicates the magnitude of the input reflection. The “scars” on the plot represent the resonance modes that have been excited. To interpret, for example, draw a vertical line on the contour plot as in Figure 38, the scars that intercepts the vertical are the excited resonance modes, and the resonance frequencies and t are found accordingly. The plots in Figure 38 provide a graphical illustration of the impact of the growing oscillation on the antenna’s input impedance. For the sinusoidal dipole, it is capable of tuning its first mode resonance frequency down to a lower frequency

compared to the straight dipole, and the slope of the first mode is steeper than the straight dipole. The trade-off is observed as that the sinusoidal dipole loses the higher operating frequency modes after 2nd resonance mode; it is seen by the diffused mode scars for the sinusoidal dipole from Figure 38.

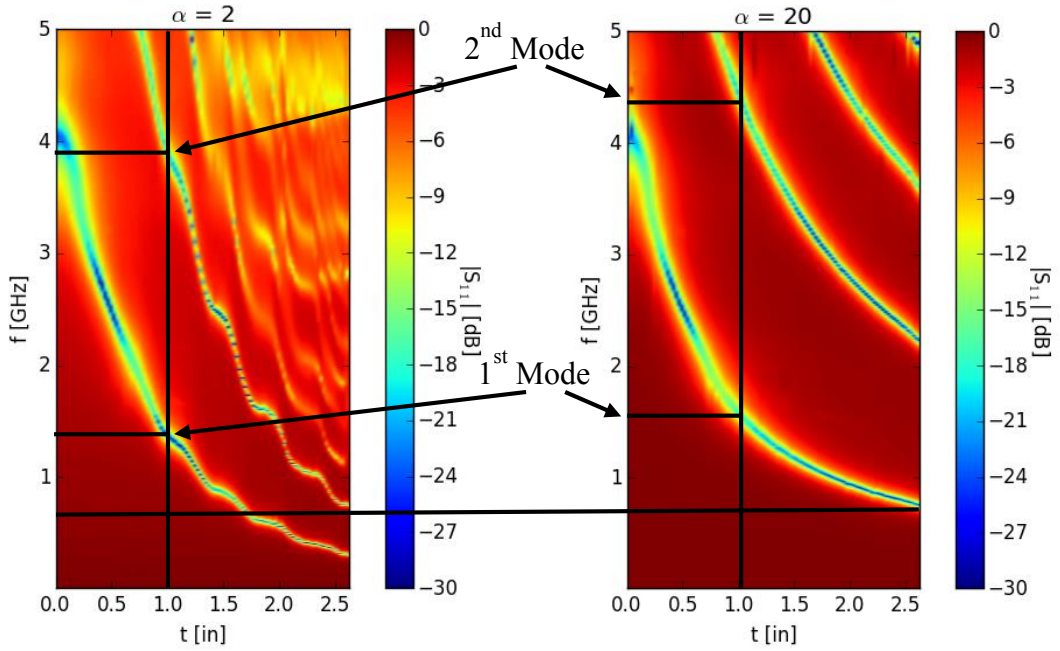

Figure 38: Log-magnitude of the Antenna's Input Reflection Coefficient; Sinusoidal Dipole (Left) and Straight Dipole (Right).

4.2 Fabrication and Verification

The fabricated antenna is shown in Figure 39. The steps taken to fabricate the composite and micro-channel are described in section 2.7. To perform input reflection and radiation pattern measurement, finite number of states are defined as in Figure 40. The impedance of the antenna was tested using a Keysight performance network analyzer (PNA). A Short Open Load Through (SOLT) calibration from 200 MHz to 5

GHz in 1 MHz steps with a 5 kHz IF bandwidth was performed. This calibration de-embeds the measurement up to the Sub-Miniature Type-A (SMA) edge-connector that is soldered to the parallel strip feed line that extends 1 cm off the edge of the composite. Once the measurement process was established, several methods to control the displacement of the liquid metal in the microvascular network is investigated. This is required to provide an accurate and repeatable displacement of the liquid metal in both channels (which need to be filled separately but equally). The final method included filling the channels with a low-dielectric low-loss heat transfer fluid (Fluorinert FC-70 Electronic Liquid by 3M), then using an appropriately-tipped syringe to inject liquid metal into the channels. The purpose of the second fluid is three-fold: first, it provides sufficient back-pressure to stabilize the flow of the semi-viscous liquid metal; second, it provides a barrier fluid to prevent oxidation; and third, it provides a method to interface additional pushing fluids that can be used for sensing, feedback, and control (this is not currently used with this antenna topology).

Figure 39: Fabricate Sinusoidal Antenna Front (Left) and Back (Right)

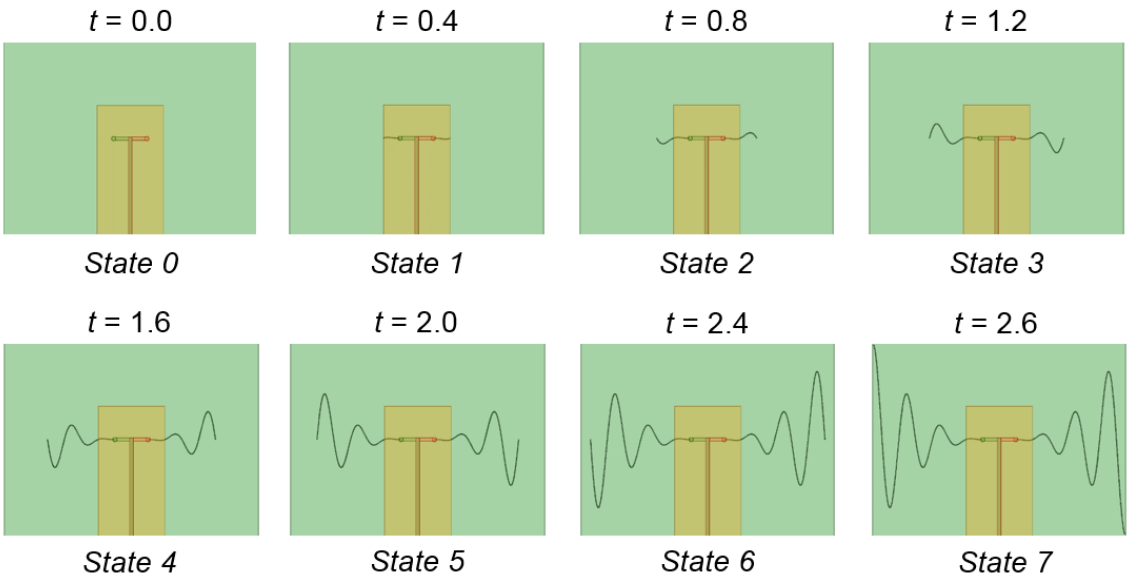

Figure 40: Sinusoidal Antenna Measured States

Figure 41 to Figure 48 are the measured input reflection data plotted against simulated data for the sinusoidal antenna. The frequency of the first mode is lowered, and more resonance modes are excited as the more liquid metal is injected in the channel which is the expected behavior of the sinusoidal antenna. Only the first mode is of interest because the trade-off made between sinusoidal dipole and straight dipole (wider frequency tuning range, but less resonance modes). The repeated measurement data for state 4 is plotted along with simulated in Figure 49. This exhaustive measurement campaign was performed to ensure the measurements were repeatable and provide a statistical basis for the uncertainty in the position of the fluid because the position of the liquid metal is judged by visual inspection. Table 6 contains the statistical data of state 4 input reflection measurement which helps to determine the accuracy of the input reflection for state 1 to state 7.

The measured radiation pattern data and simulated data for the first resonance mode are plotted together from Figure 50 to Figure 57. A dipole like radiation pattern is expected for the sinusoidal antenna because meandering a straight dipole trace helps with input impedance matching, but the radiation pattern is perturbed slightly because of phase cancellation between meandered traces.

Resonance Mode	Resonance Frequency		Bandwidth	
	Mean (GHz)	Standard Deviation (MHz)	Mean (MHz)	Standard Deviation (MHz)
First	0.7661	3.87	70.1	1.66
Second	2.1163	16.81	77.7	3.43
Third	3.1648	25.01	134.5	3.57

Table 6: Statistical Data of Sinusoidal Antenna State 4 Input Reflection Measurement

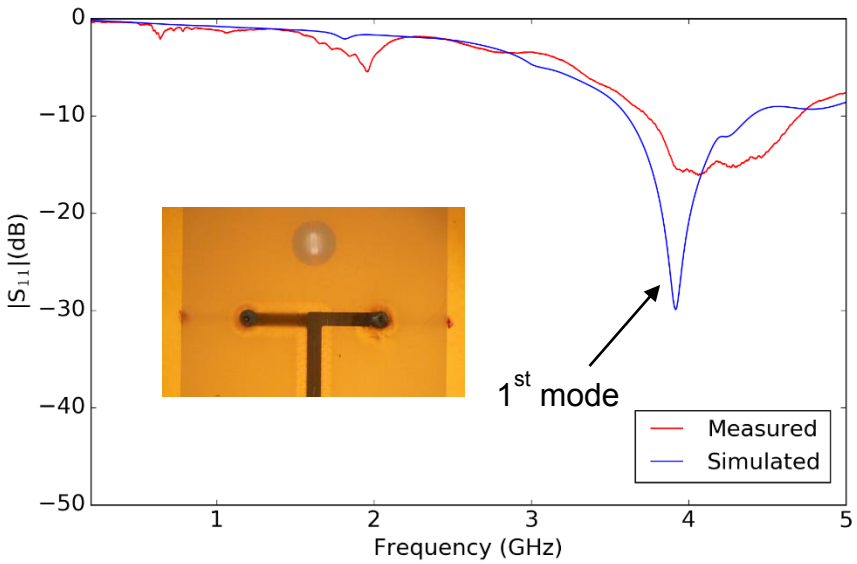

Figure 41: Sinusoidal Antenna State 0 |S11|

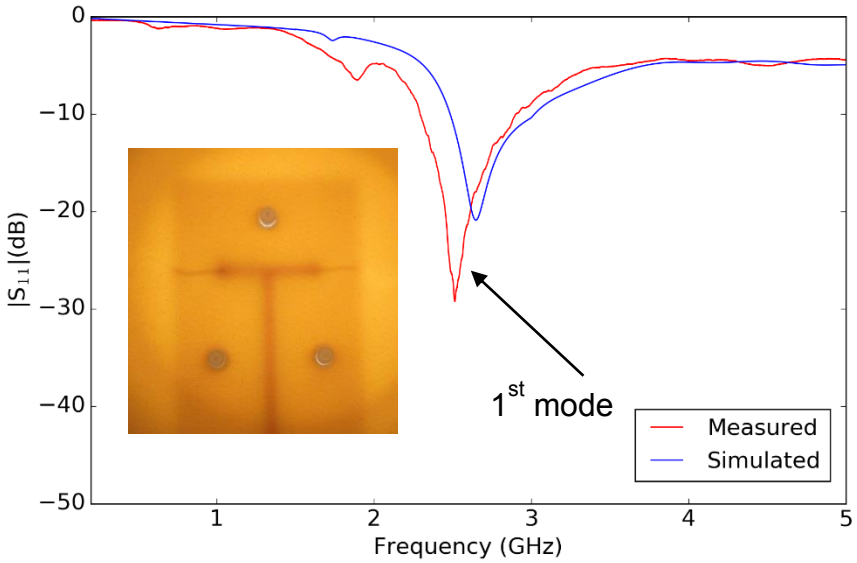

Figure 42: Sinusoidal Antenna State 1 |S11|

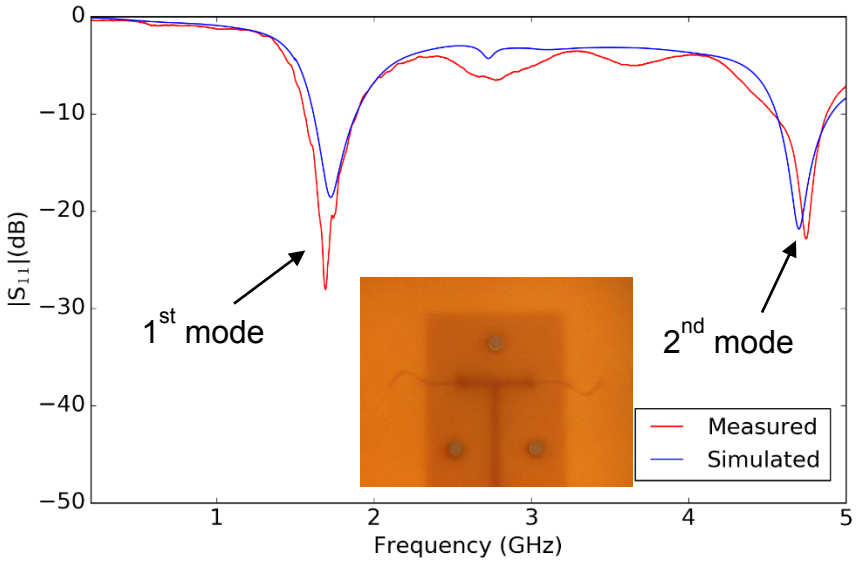

Figure 43: Sinusoidal Antenna State 2 |S11|

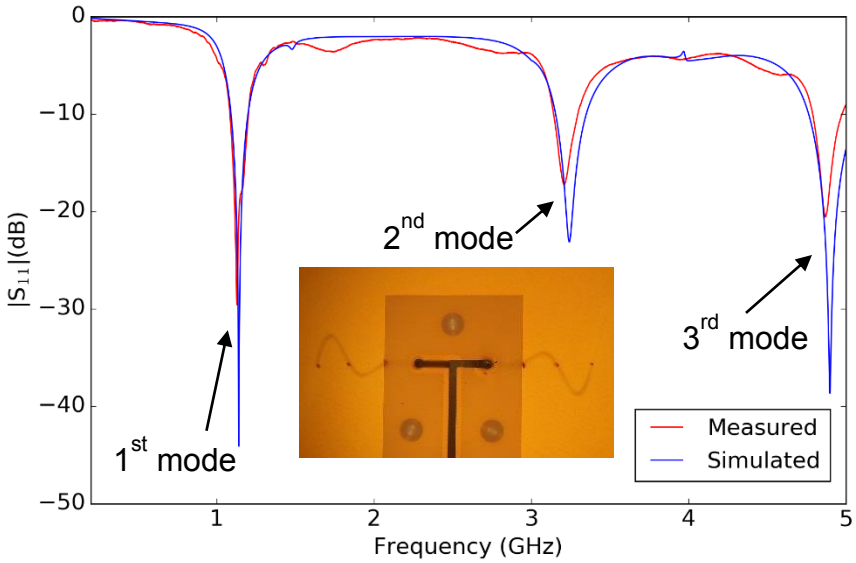

Figure 44: Sinusoidal Antenna State 3 |S11|

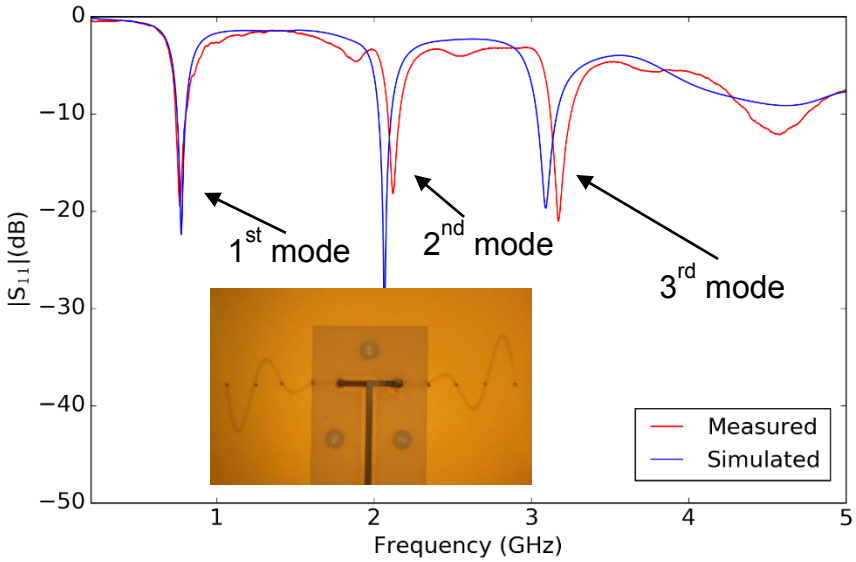

Figure 45: Sinusoidal Antenna State 4 |S11|

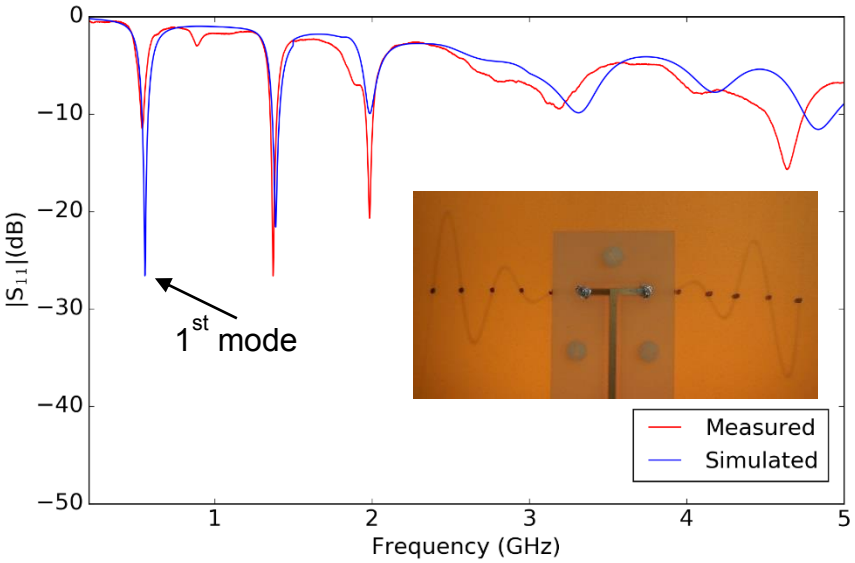

Figure 46: Sinusoidal Antenna State 5 |S11|

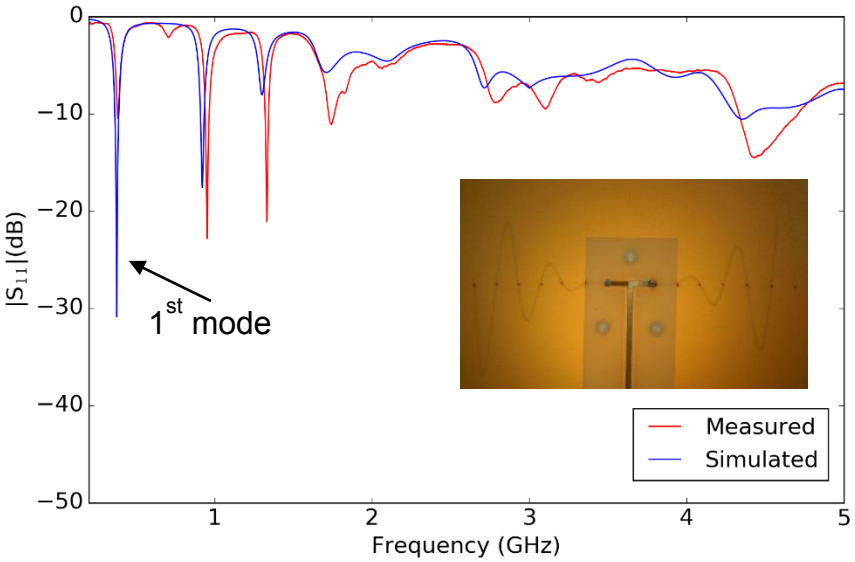

Figure 47: Sinusoidal Antenna State 6 |S11|

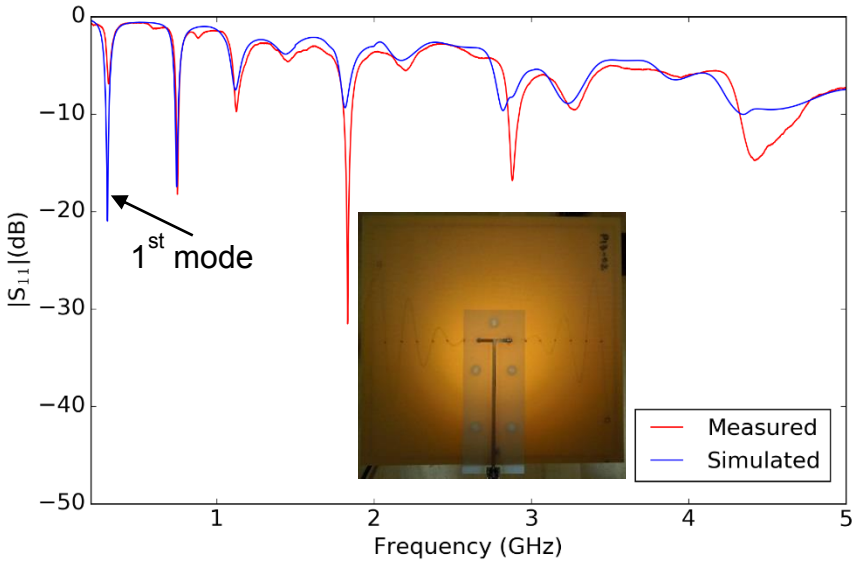

Figure 48: Sinusoidal Antenna State 7 |S11|

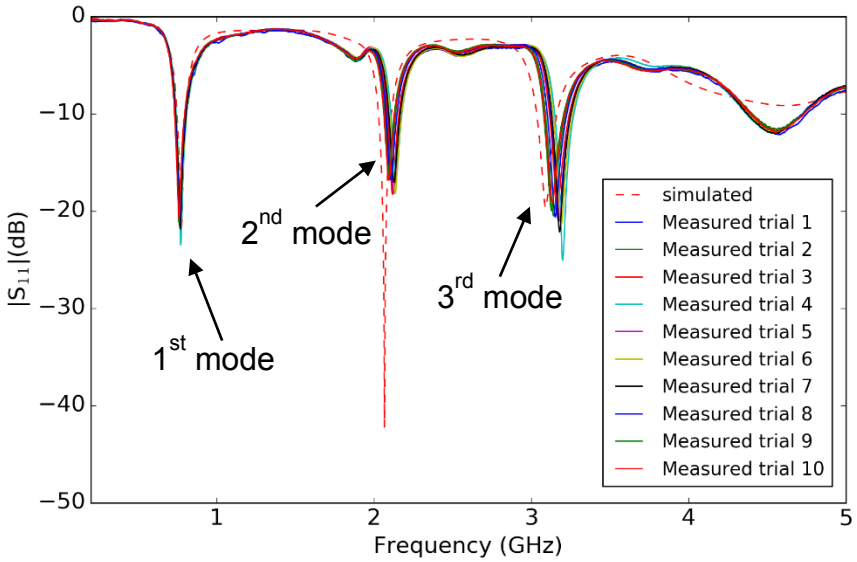

Figure 49: Sinusoidal Antenna State 4 Repeated |S11| Measurement

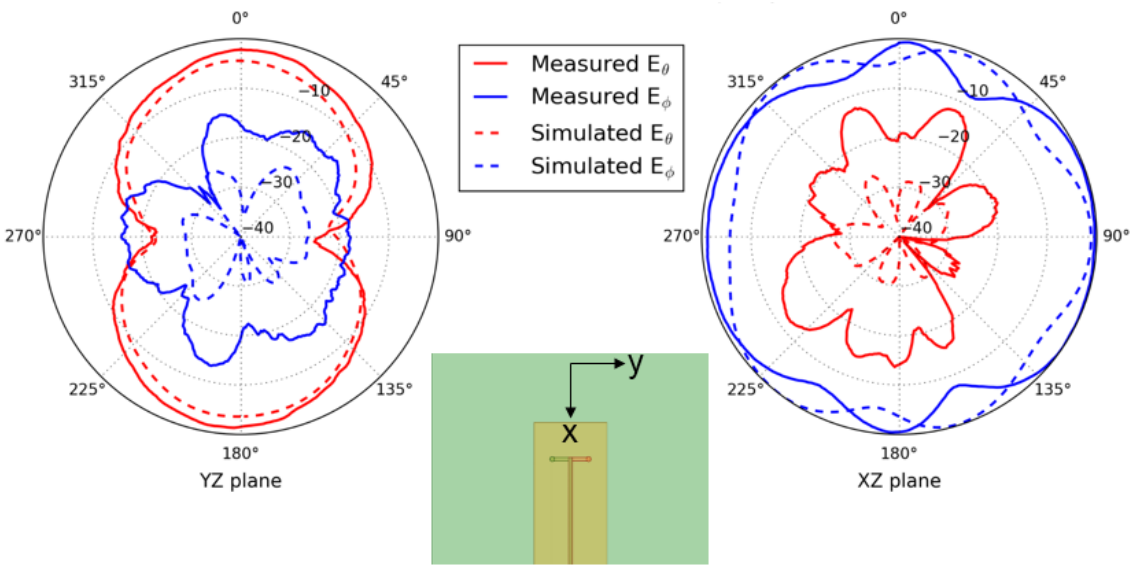

Figure 50: Sinusoidal Antenna State 0 Pattern Measurement

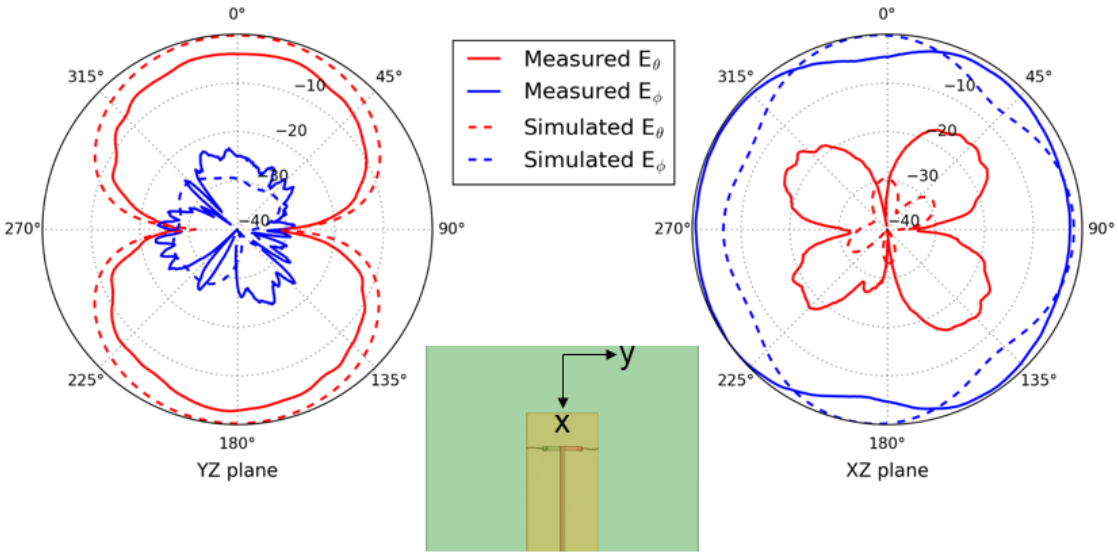

Figure 51: Sinusoidal Antenna State 1 Pattern Measurement

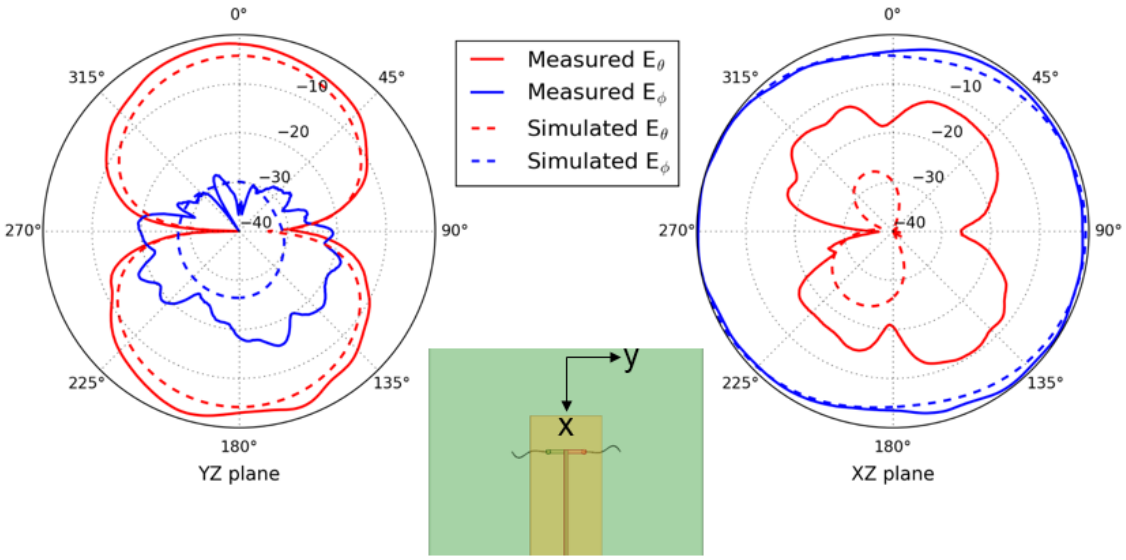

Figure 52: Sinusoidal Antenna State 2 Pattern Measurement

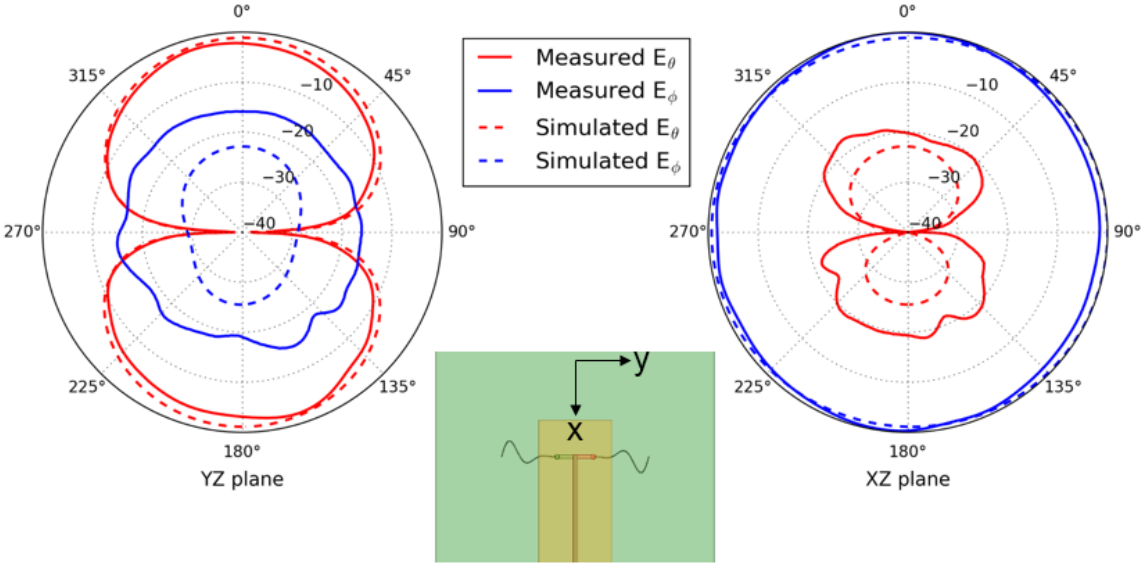

Figure 53: Sinusoidal Antenna State 3 Pattern Measurement

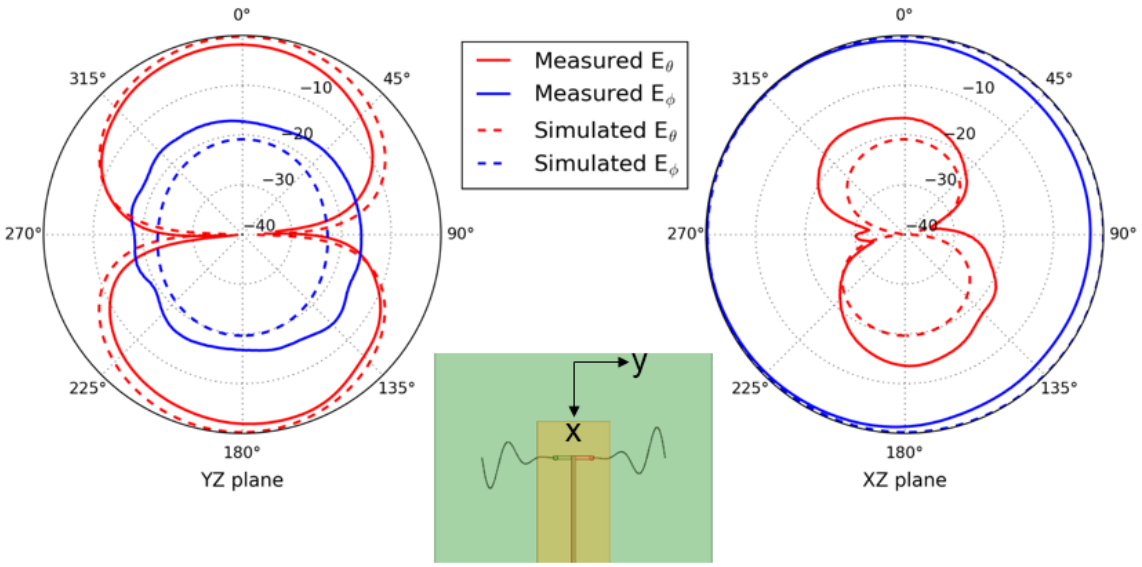

Figure 54: Sinusoidal Antenna State 4 Pattern Measurement

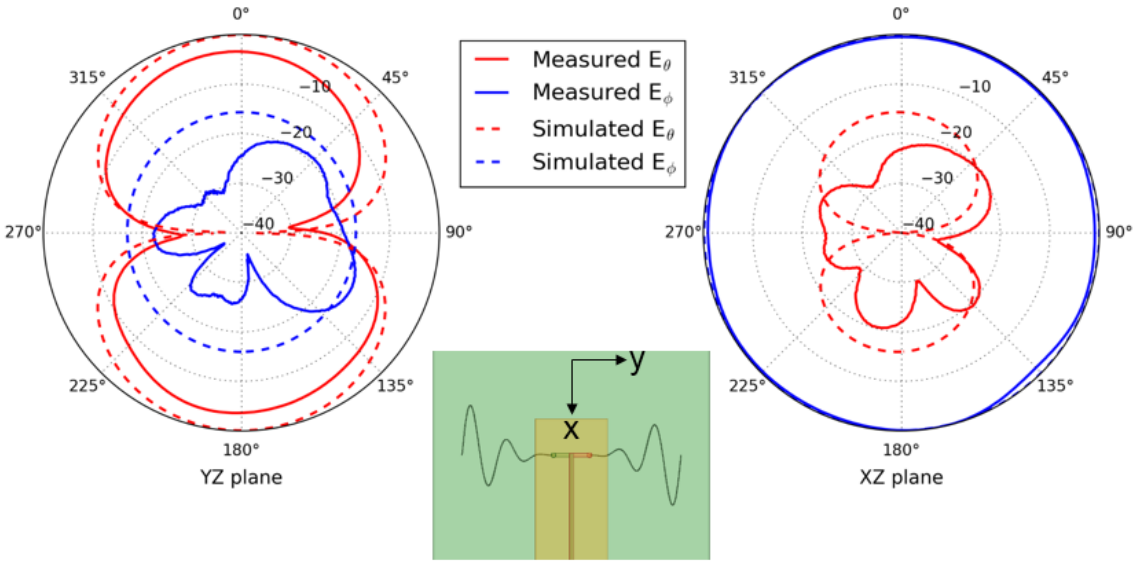

Figure 55: Sinusoidal Antenna State 5 Pattern Measurement

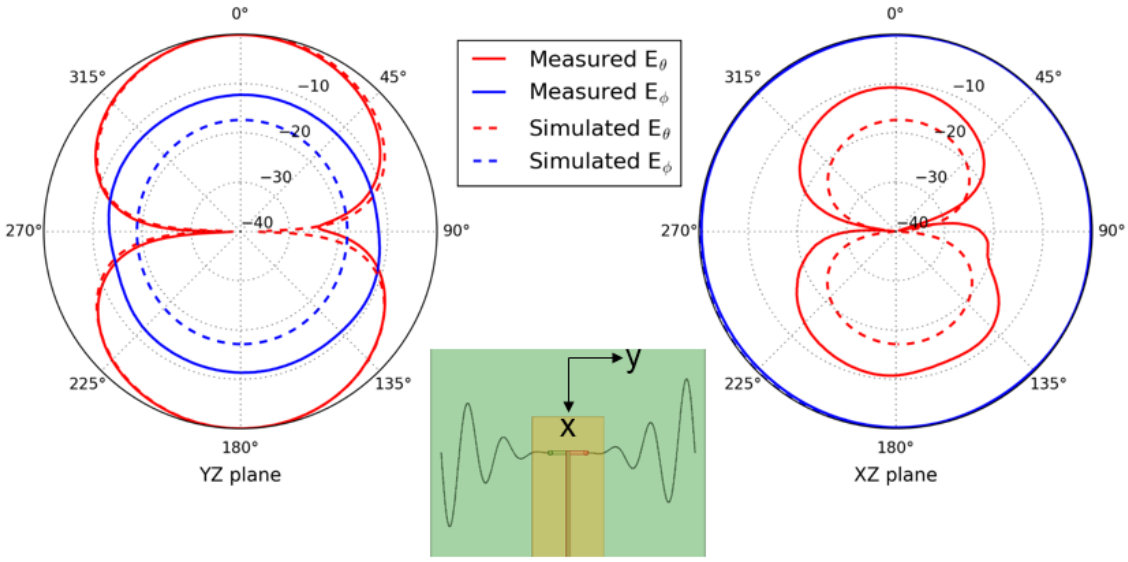

Figure 56: Sinusoidal Antenna State 6 Pattern Measurement

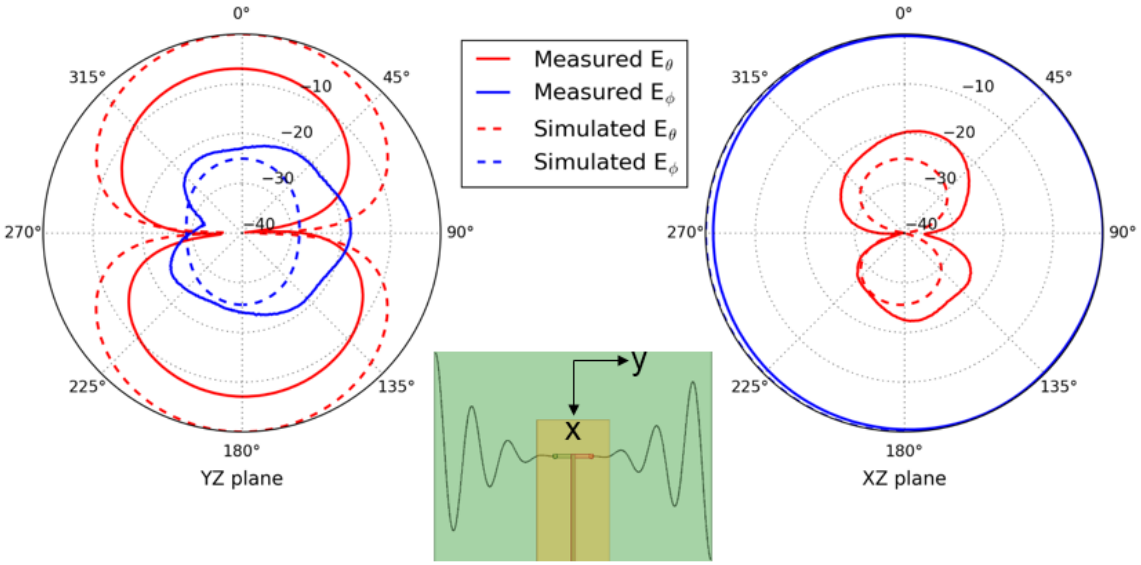

Figure 57: Sinusoidal Antenna State 7 Pattern Measurement

CHAPTER 5

POLARIZATION RECONFIGURABLE MICROSTRIP CROSS PATCH ANTENNA

5.1 HFSS Simulation

The objective of the cross patch antenna is to provide performance metrics for difference switch mechanisms. The cross patch antenna radiates in the same way as the trandition patch antenna described in section 2.5. The major difference is that two resonance modes have been excited to make the cross patch antenna a dual polarized antenna. Then the arms of the cross patch is cut to stop the excitation. In this way, when EGaIn (green trace in Figure 58) re-establish the connection between arms and the center conductor, resonance mode with different polarization can be selectively excited. The connection can also be made by using PIN diodes. A different switch mechanism is to use dielectric fluid as a way to provide impedance matching if the connection of the arms is thought of as a transmission line problem. All three different switching mechanisms are placed side by side in Figure 59. The simulated radiation efficiency is compared in Table 7. The efficiency data for cross patch antenna with PIN Diode and Dielectric Fluid as switching mechanism is extracted from [15]. The main advantage of using PIN diode is the fast switching speed, but the internal resistance of the PIN diode dissipates energy and brings down the radiation efficiency. The dielectric fluid is currently easier to control in a microfluidic channel compared to EGaIn, and using dielectric fluid as a switch has higher efficiency compared to using PIN diode. The radiation efficiency is boosted up to 80% when EGaIn is used. The measured radiation

efficiency data for all three antenna is not avaiable at this moment, but the simulated data can be considered as a upper bound of the radiation efficiency[15].

Switching Mechanism	PIN Diode	Dielectric Fluid	EGaIn
Radiation Efficiency	10%	22%	80%
Advantage	Fasting Switching	Easy Fluid Control	High Radiation Efficiency

Table 7: Comparison of Radiation Efficiency with Different Switching Mechanism

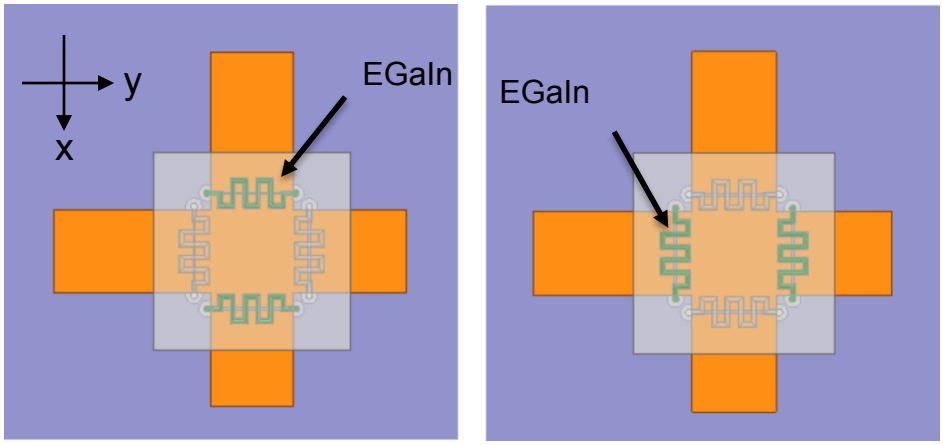

Figure 58: Cross Patch Antenna X-pol (Left) and Y-pol (Right)

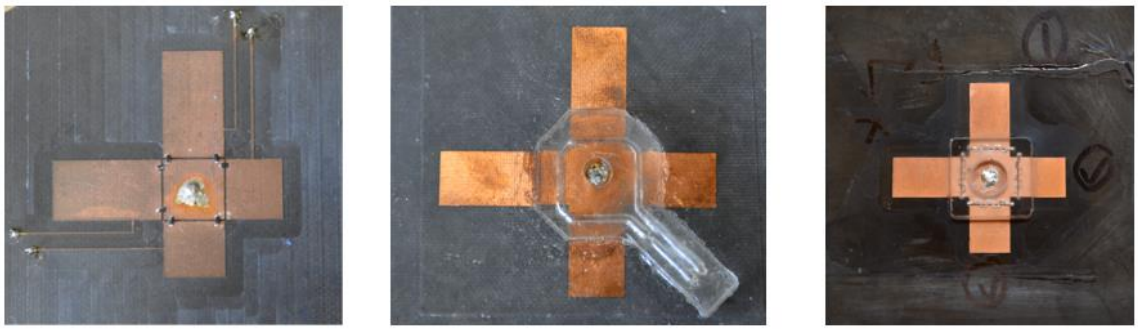

Figure 59: Cross Antenna Enabled by Different Switching Mechanisms

5.2 Fabrication and Verification

The cross patch antenna enabled by EGaIn has gone through four major iterations shown in Figure 60. Iteration 1 has diffculty testing the antenna because one continous fluidic channel is cast on top of the antenna. It takes many trails to get the EGaIn positioned correctly. Iteration 2 has drilled hole in the back that directly connect to the channel on the front side. Iteration 3 brings the feed channel to the edge of the back side of the antenna because the EGaIn shorts to the ground if EGaIn leaks out of the channel in iteration 2. The epoxy on the front and back side of the antenna in iteration 3 is cured seperately because of the 3D channel cannot be cast to the front and back side at the same. It was suspected that EGaIn is not making good connection between the arms in iteration 3, and iteration 4 uses meandering channel like the one used for the slot antenna to address the connection issue. The input reflection, input impedance, and radiation pattern data (from Figure 61 to Figure 64)is from iteration 3.

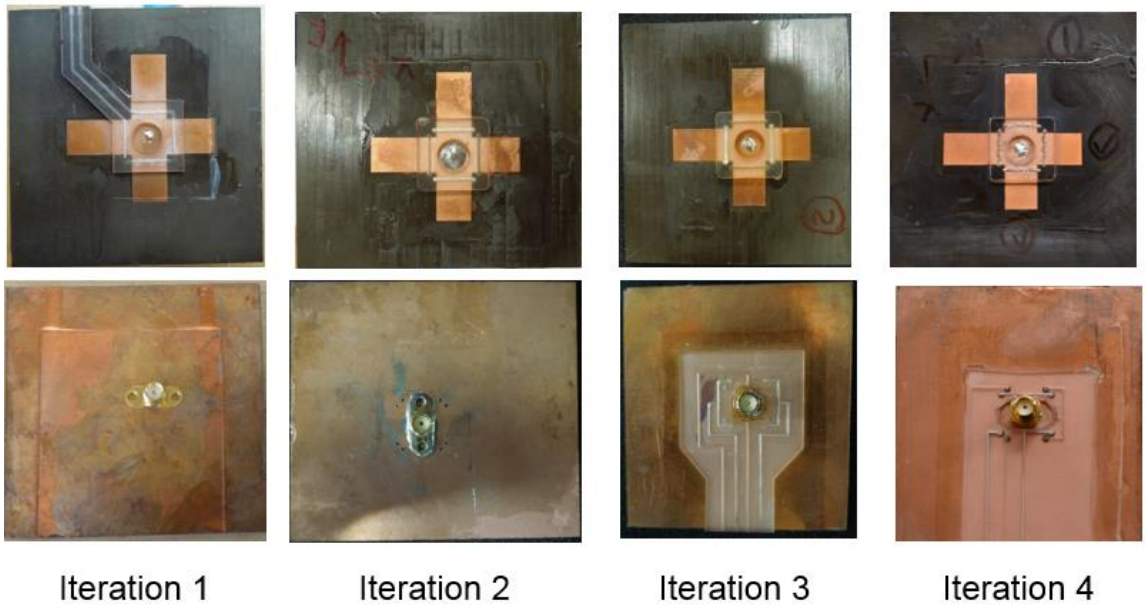

Figure 60: Four Versions of Fabricated Cross Patch Antenna

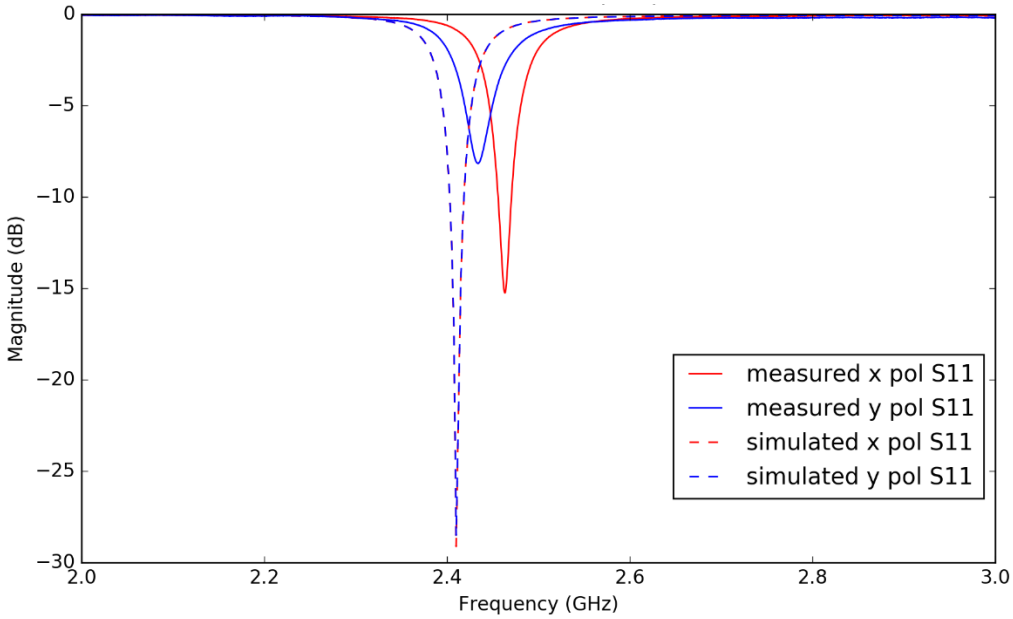

Figure 61: Cross Patch Antenna Input Reflection

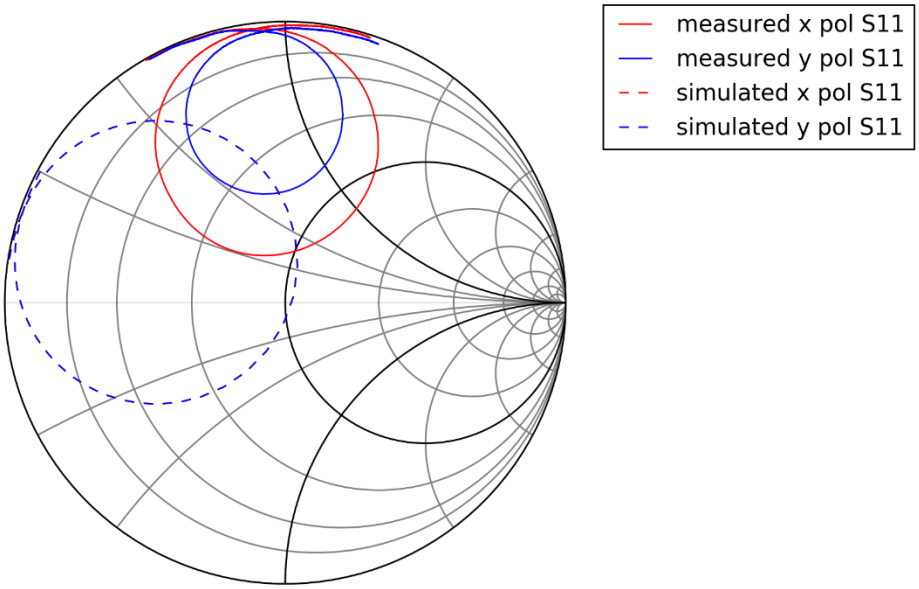

Figure 62: Cross Patch Antenna Input Impedance

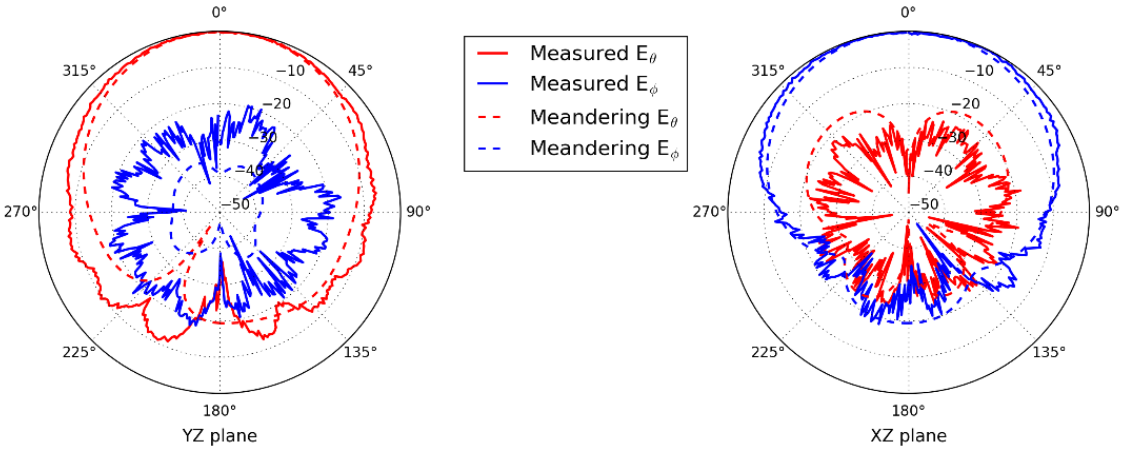

Figure 63: Cross Patch Antenna Radiation Pattern, Y-pol

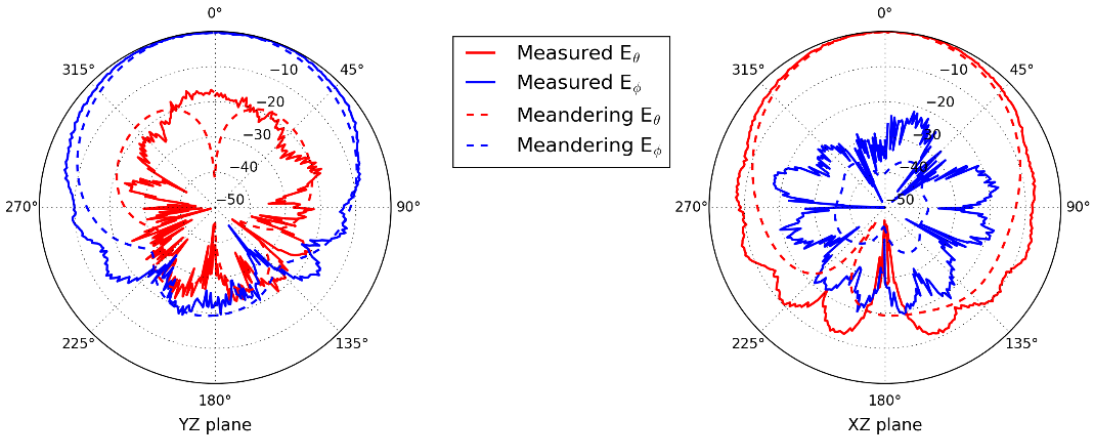

Figure 64: Cross Patch Antenna Radiation Pattern, X-pol

CHAPTER 6

CONCLUSION

6.1 Conclusion

The circular SIW cavity backed slot antenna use EGaIn to flow in a microfluidic channel to change its polarization by changing the position of the aperture. It is mainly to demonstrate the automation of EGaIn and low cost PCB integration. The challenges are associated with fluidic channel construction and bonding and fluid actuation in the channel. The fluidic actuation can be improved by adding more sensor in the sensor network to predict and pinpoint the position of EGaIn.

The frequency reconfigurable sinusoidal dipole antenna that uses EGaIn as a radiating element to change its resonance frequency by contracting and expanding the length of EGaIn. The objective of the sinusoidal antenna is to provide frequency tunability over a wide bandwidth and to minimize antenna installation area and/or weight for the use on an aircraft. Moving EGaIn in the channel was problematic because it was challenging to accurately locate EGaIn in the channel. If a sensor network like the one built for the slot antenna were to add to the sinusoidal dipole antenna, it will make the antenna more usable in a practical sense. Different methods of moving EGaIn like the one described in [16] is well worth exploring to improve the actuation.

The polarization reconfigurable cross patch antenna that uses EGaIn as a switch to alter its polarization. It provides performance metrics for difference switch mechanisms (PIN diode, Dielectric fluid, EGaIn). The main advantage of using PIN diode is the fast switching speed, but the internal resistance of the PIN diode dissipates

energy and brings down the radiation efficiency. The dielectric fluid is currently easier to control in a microfluidic channel compared to EGaIn, and using dielectric fluid as a switch has higher efficiency compared to using PIN diode. The radiation efficiency is boosted up to 80% when EGaIn is used.

This thesis investigated reconfigurable antennas enabled by non-toxic liquid metal, Eutectic Gallium Indium (EGaIn) and demonstrated that the integration of emerging additive manufacturing techniques and liquid metal fluidic systems in the design of reconfigurable antennas. All three antennas have been built to demonstrate the utility of EGaIn, capability of additive manufacturing techniques, integration of an antenna to a low cost PCB with readily available fabrication process and high strength multifunctional structural composite.

REFERENCES

[1] R. R. Ramirez and F. D. Flaviis, "A mutual coupling study of circular polarized microstrip antennas with applications to diversity combining mobile communications," in *Antennas and Propagation Society International Symposium, 2001. IEEE*, 2001, pp. 244-247 vol.3.

[2] H. Aissat, L. Cirio, M. Grzeskowiak, J. M. Laheurte, and O. Picon, "Reconfigurable circularly polarized antenna for short-range communication systems," *IEEE Transactions on Microwave Theory and Techniques*, vol. 54, pp. 2856-2863, 2006.

[3] X. Wang, H. Zhao, Y. Niu, and Y. Zhang, "MEMS dual-band frequency and polarization reconfigurable microstrip antenna," in *Geoscience and Remote Sensing (IITA-GRS), 2010 Second IITA International Conference on*, 2010, pp. 51-53 vol 1.

[4] W. M. Haynes, *CRC handbook of chemistry and physics* 96th (Internet Version 2016) ed. Boca Raton, FL: CRC Press/Taylor and Francis, 2016.

[5] M. D. Dickey, "Emerging applications of liquid metals featuring surface oxides," *ACS Applied Materials & Interfaces*, vol. 6, pp. 18369–18379, Oct 6 2014.

[6] M. R. Khan, G. J. Hayes, S. Zhang, M. D. Dickey, and G. Lazzi, "A pressure responsive fluidic microstrip open stub resonator using a liquid metal alloy," *IEEE Microwave and Wireless Components Letters*, vol. 22, pp. 577-579, 2012.

[7] M. Kelley, C. Koo, H. Mcquilken, B. Lawrence, S. Li, A. Han, *et al.*, "Frequency reconfigurable patch antenna using liquid metal as switching mechanism," *Electronics Letters*, vol. 49, pp. 1370-1371, 2013.

[8] C. Koo, B. E. LeBlanc, M. Kelley, H. E. Fitzgerald, G. H. Huff, and A. Han, "Manipulating liquid metal droplets in microfluidic channels with minimized skin residues toward tunable rf applications," *Journal of Microelectromechanical Systems*, vol. 24, pp. 1069-1076, 2015.

[9] D. M. Pozar, *Microwave engineering*, 4th ed. Hoboken, NJ: Wiley, 2012.

[10] J. Ajioka, "On the conceptual utility of current flow lines in waveguides," *IEEE Transactions on Antennas and Propagation*, vol. 34, pp. 219-227, 1986.

[11] K. Chang, *RF and microwave wireless systems*. New York: Wiley, 2000.

[12] W. L. Stutzman and G. A. Thiele, *Antenna theory and design*, 3rd ed. Hoboken, NJ: Wiley, 2013.

[13] C. A. Balanis, *Antenna theory : analysis and design*, 3rd ed. Hoboken, NJ: John Wiley, 2005.

[14] D. J. Hartl, G. H. Huff, H. Pan, L. Smith, R. L. Bradford, G. J. Frank, *et al.*, "Analysis and characterization of structurally embedded vascular antennas using liquid metals,", vol. 9803 pp. 980333-980333-9, 2016.

[15] J. D. Barrera and G. H. Huff, "A fluidic loading mechanism in a polarization reconfigurable antenna with a comparison to solid state approaches," *IEEE Transactions on Antennas and Propagation*, vol. 62, pp. 4008-4014, 2014.

[16] S.-Y. Tang, Y. Lin, I. D. Joshipura, K. Khoshmanesh, and M. D. Dickey, "Steering liquid metal flow in microchannels using low voltages," *Lab on a Chip*, vol. 15, pp. 3905-3911, 2015.